博　士　論　文

Decadal Variability of Antarctic Sea Ice Variability revealed by Satellite Observation and Coupled General Circulation Model

(衛星観測と結合大循環モデルにより得られた南極海海氷の十年規模変動)

A dissertation submitted in partial fulfillment of
the requirements for the degree of

Doctor of Environmental Earth Science

Graduate School of Environmental Science, Hokkaido University
北海道大学大学院環境科学院

Chevooruvalappil Bajish Chandran
チボールワラピル バジシュ チャンドラン

August, 2013

Abstract

In the last 30 years, contrary to the Arctic sea ice rapid decrease, the Antarctic sea ice extent has been showing an increasing trend, with significant regional scale increase at the Ross Sea sector and decrease at Bellingshausen Sea. This long-term Antarctic sea ice variability (∼10-30 years) is difficult to examine due to the limitation in the satellite observation record and its mechanism has not been sufficiently addressed yet. In order to study the decadal variability in the Antarctic sea ice and the processes driving it, this study examined the relationship between ice, ocean and atmosphere using a high resolution coupled ocean-atmosphere-ice model (CFES) along with observational data derived from satellite.

The observational records of sea ice have revealed a circumpolar variability of sea ice edge (SIE) on decadal time scale (11-16 years). Sea surface temperature (SST) observations and southern annular mode (SAM) record also showed variation on similar timescales with warm (cool) anomaly corresponding to retreat (extension) of SIE at negative (positive) SAM. These coupled relationships are also confirmed from our model study where the leading modes of sea ice concentration (SIC) is circumpolar pattern with a dominant time scale of 12-17 years and the leading mode

of SST also has similar pattern with SIC showing a high degree of inverse correlation. The modeled SAM significantly correlates with the leading modes of both SIC and SST. The model and observation also showed a good quantitative with 1°C decrease (increase) of model SST corresponding to 1.4 degree extension (retreat) of SIE which is slightly larger than the observation.

The oceanic variability especially in the SST sets the decadal variability in the Antarctic sea ice. The atmosphere, especially SAM, initiates the decadal sea ice variability with related wind anomalies induce Ekman currents in the mixed layer which produce SST anomalies with the upwelling of the warmer subsurface water at a decadal time scale (14-18 years). The decadal SAM and oceanic variability are coupled through dynamic and thermodynamic feedback. Therefore, the natural oceanic decadal variability its impact to the atmosphere is the key in the coupled ice-ocean-atmosphere system.

Contents

Chapter 1

Introduction

Antarctic sea ice is important for its role in the global and regional climate through its ice-albedo feedback mechanism, thermal insulating effect between the ocean and the atmosphere, and deep water formation at the polynyas [e.g., *Walsh*, 1983; *Curry et al.*, 1995; *Holland et al.*, 2001; *Ohshima et al.*, 2013]. Recent satellite records revealed that unlike the Arctic, the total Antarctic sea ice extent shows a slightly increasing trend, with regional variations of increase at the Ross Sea sector and decrease at the Bellingshausen Sea sector [*Zwally et al.*, 2002; *Cavalieri and Parkinson*, 2008; *Parkinson and Cavalieri*, 2012] (Fig. 1.1 and see Fig 1.2 for representations of geographic locations). This long-term increasing trend in Antarctic sea ice has not been clearly reproduced by the IPCC-class models to date [e.g., *Landrum et al.*, 2012] and the mechanism of its long-term variability has not been sufficiently addressed yet.

There are distinct climate modes of variability acting on the high-latitude region of the Southern Hemisphere [*Yuan and Li*, 2008] and these modes have primary role in defining the patterns of sea ice variability on various time scales. Southern Annular

mode (SAM; Antarctic Oscillation AAO) is one of the dominant climate modes. It is represented by annular shaped zonally symmetric out of phase pressure anomalies over the Antarctic continent and the mid latitude region [*Gong and Wang*, 1999; *Thompson et al.*, 2000]. Using a numerical model, *Hall and Visbeck* [2002] explained positive SAM is associated with stronger westerly with increased ice transport towards the north resulting in the increase of total sea ice as a circumpolar mode. However, *Lefebvre et al.* [2004] showed that, on inter-annual timescale SAM has a non annular response on sea ice with opposing effects with sea ice decrease for positive SAM at Weddell sea and Antarctic peninsula region and sea ice increase at Ross sea and Amundsen sea region for positive SAM. The negative pressure anomalies extending over the Amundsen Sea which consequently induces warm northerly (cold southerly) winds to blow over the Antarctic peninsula (Ross/Amundsen Seas) gives rise to the anomalous sea ice concentration (SIC) dipole. Moreover, the ice drift caused by the anomalous wind stress and Ekman transport reinforces the SIC dipole [*Lefebvre et al.*, 2004; *Liu et al.*, 2004; *Lefebvre and Goosse*, 2005].

Pacific South American (PSA) pattern is also dominant climate mode in the polar/sub polar region on the inter-annual scale. It is attributed to the Rossby wave propagation to the southern high latitudes as a response to the El Niño - Southern Oscillation (ENSO) [*Yuan*, 2004] with anomalous high pressure center in the Amundsen sea. The PSA SIC anomalies are alternating pattern with increase at Weddell sea and Antarctic peninsula region and decrease at Ross sea and Amundsen sea region [*Yuan*, 2004; *Liu et al.*, 2004].

The influence of both the SAM and PSA on Antarctic SIC anomalies has been

examined in a number of observational and modeling studies [e.g., *Yuan and Martinson*, 2000; *Hall and Visbeck*, 2002; *Lefebvre et al.*, 2004; *Liu et al.*, 2004; *Stammerjohn et al.*, 2008; *Yuan and Li*, 2008; *Udagawa et al.*, 2009]. *Udagawa et al.* [2009] showed that PSA was the predominant climatic mode when the sea ice anomaly propagates eastwards (like Antarctic circumpolar wave [*White and Peterson*, 1996]) and in the non propagating years SAM was dominant. The PSA SIC anomalies are qualitatively similar to those described for the non-annular SAM response [*Liu et al.*, 2004] due to the existence of height anomalies over the Amundsen sea but are of opposing sign [e.g., *Yuan and Martinson*, 2000; *Liu et al.*, 2004; *Yuan and Li*, 2008]. However, these analysis are mostly concerning on the sea ice behavior on the inter-annual time scale, partly due to the short record length of satellite observations, and studies of patterns and dynamics on the decadal or longer-time scales are not enough.

Over the recent several decades from the 1970s, SAM is known to shift to positive phase [e.g., *Thompson and Solomon*, 2002; *Visbeck*, 2009], although the sea ice increase is not sufficiently explained by the combinations of responses to the dominant modes of variability [*Liu et al.*, 2004; *Stammerjohn et al.*, 2008]. In addition, SAM has a prominent variability on the qausi-decadal (8-16 year) time scale from the observational records [*Yuan and Yonekura*, 2011]. This quasi-decadal SAM is accompanied with a circumpolar SST pattern, with cooler (warmer) SST anomaly around the Antarctic coast for high (low) SAM years. However, the response of sea ice on this time scale is not sufficiently studied both for observation and models. There is few evidence for offshore pack ice, but the observational records of the land fast-ice in the Indian ocean sector indicates a presence of stable–break-up periodicity of around 20

years [*Ushio*, 2006]. Some model [e.g., *Holland et al.*, 2005; *Goosse et al.*, 2008] studies hint that SAM may have larger influence on the sea ice variability than PSA/ENSO on decadal to multi-decadal time scale. Most of the 20th century runs of IPCC models (CMIP3), including green house gases and ozone effects, revealed the quasi-decadal variability in SAM, whereas only some models could reveal the decadal variability in SST. *Yuan and Yonekura* [2011] suggests the quasi-decadal variability is a natural variability which might be primarily caused by ocean dynamics. To understand the behavior of decadal variabilities in the ocean and thereby its impact on sea ice, it is necessary to differentiate the dynamics inherent to the coupled ocean-atmosphere-sea ice system from the conditions with anthropogenic and/or geological forcing. Hence the purely natural variability of the atmosphere-ocean-sea ice system needs to be understood.

In the present study we investigate the decadal variability in sea ice and its relationship with atmosphere and ocean. From around 30-year observational data of SIC and SST, dominant pattern of decadal/long-term variability are studied, especially in relation to SAM. Dominant modes revealed in a coupled atmosphere-ocean-sea ice model run (longer than 100 year) are then examined to compare and explain the observed patterns by natural variability of climate system. Interaction between ocean and atmosphere variabilities are studied from model dynamics.

In chapter 2, we describe the data and methods used and also verify the model fidelity with that of the observations. The characteristics on the decadal variability in Antarctic sea ice is discussed in chapter 3. Chapter 4 discusses the mechanism of the decadal variability in the Antarctic sea ice by analyzing the temperature change

of ocean interior and upwelling velocity. We present the discussion on the results of our study in chapter 5 and finally the conclusions are presented in chapter 6.

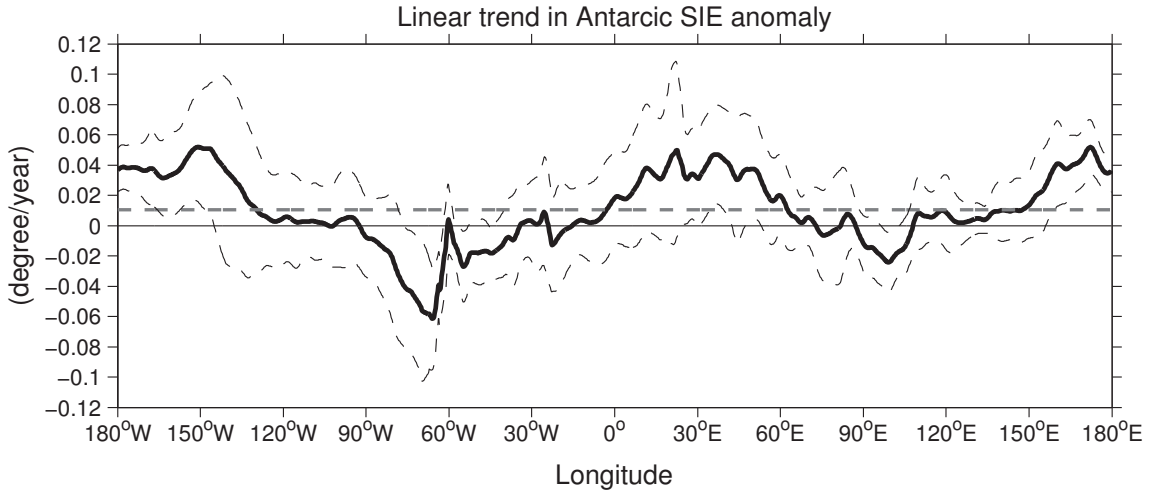

Figure 1.1: The linear trend of the sea ice edge location as a function of longitude (solid black line) from 1979-2010 derived from satellite observation. Dashed black lines represents the 95% confidence intervals of the zonal trend. The dashed grey line indicate the mean trend. Positive trend indicates areas of ice edge expansion and negative trend indicate retreat. Sea ice edge is defined by the equatorward latitudinal position of 30% isopleth of sea ice concentration [*Yuan and Martinson*, 2000].

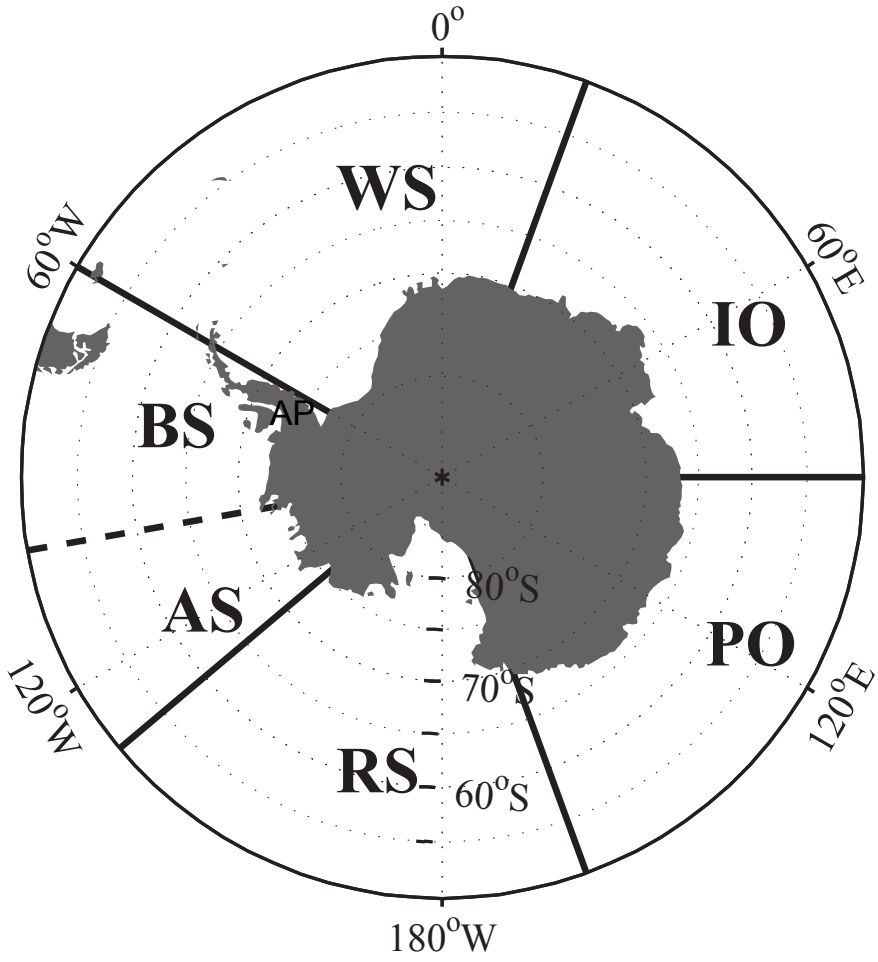

Figure 1.2: Sectors of the Southern Ocean. These are Weddell sea (WS; 60°W-20°E), the Indian Ocean (IO; 20°E-90°E), the Pacific Ocean (PO; 90°E-160°E), the Ross sea (RS; 160°E-130°W) and Amundsen-Bellingshausen seas (AS&BS; 130°W-60°W). The Antarctic peninsula (AP) region is defined as the oceanic region from 80°W westward of Antarctic peninsula towards 50°W in the east.

Chapter 2

Antarctic sea ice and fidelity of coupled general circulation model

2.1 Data and methods

In the Antarctic, the sea ice data prior to the satellite record are sparse. Historical record of sea ice extent are the one kept by Antarctic whalers since the 1930s on the location of all whales caught. Because whales tend to congregate near the sea ice edge to feed, their locations could be a proxy for the ice extent. However, only the satellite record is considered sufficiently reliable for studying Antarctic sea ice trends. To study the realistic modes of sea ice variability and validate the model results, satellite sea ice data were examined. Since ocean and atmosphere play vital roles in the sea ice variability, relationships are studied with satellite derived SST dataset and SAM index. The 120 year CGCM integration, which is much longer than the observational data, enables dynamical examination and also augments statistical

significance of our results. The model provides data of physically consistent ice-ocean-atmosphere coupled variability despite its uncertainties in physical parameterizations of subgrid processes, allowing more spatial and temporal coverage complementary to the observational data.

2.1.1 Observations

Since 1979, satellites have provided a continuous, nearly complete record of Earth's sea ice. The most valuable datasets come from satellite sensors that observe microwaves emitted by the ice surface because, unlike visible light, the microwave energy radiated by the sea ice surface passes through clouds and can be measured even at night. The continuous sea ice record began with the Nimbus-7 Scanning Multichannel Microwave Radiometer (October 1978-August 1987) and continued with the Defense Meteorological Satellite Program Special Sensor Microwave Imager (1987 to present). The Advanced Microwave Scanning Radiometer for EOS on NASA's Aqua satellite has been observing sea ice since 2002 [http://earthobservatory.nasa.gov/Features/SeaIce/].

The monthly satellite SIC data in the southern ocean, from the National Snow and Ice Data Center (NSIDC) were used in this study. This SIC data set was derived using measurements from the Scanning Multichannel Microwave Radiometer (SMMR) on the Nimbus-7 satellite and from three Special Sensor Microwave/Imager (SSM/I) sensors on the Defense Meteorological Satellite Program's (DMSP) -F8, -F11, and -F13 satellites. The data set has been generated using the Advanced Microwave Scanning Radiometer - Earth Observing System (AMSR-E) Bootstrap Algorithm [*Comiso*, 2000]. Data are gridded on the SSM/I polar stereographic grid (25 x 25 km) from

1979 to 2010.

As for SST data set we use NOAA Optimum Interpolation (OI) SST version 2 (v.2) monthly fields. The OI SST analysis is produced weekly on a 1° x 1° grid. The analysis uses in-situ and satellite SST along with SST simulated by sea-ice cover. Before the analysis is computed, the satellite data is adjusted for biases using the method of *Reynolds* [1988] and *Reynolds and Marsico* [1993]. The OI SST v.2 monthly fields are derived by a linear interpolation of the weekly OI SST v.2 fields to daily fields and then averaging the daily values over a month. The monthly fields are in the same spatial resolution (1° x 1°) as the weekly fields from 1982-2010. The OI v.2 analysis has a modest improvement in the bias correction and also uses an improved climatological sea ice to SST conversion algorithm that better fits the in-situ data from COADS-E (enhanced COADS) [*Reynolds et al.*, 2002].

Since the main focus of this study is related to variability of annular pattern, the atmospheric condition is represented by monthly mean SAM index from 1979-2010 from Climate Prediction Center (CPC). Monthly SAM indices are constructed by projecting the monthly mean 700-hPa height anomalies onto the leading EOF mode. Time series are normalized by the standard deviation of the monthly index. The high index polarity of SAM are characterized by negative height anomalies over the pole surrounded by positive height anomalies at the mid latitudes.

2.1.2 Model description

To investigate the sea ice behavior and its relationship with the oceanic and atmospheric variabilities, a coupled General Circulation Model is indispensable in exam-

ining their dynamical balance. The model used in this study is the CGCM for the Earth Simulator (CFES), which consists of the AFES3 (AGCM for the ES) [*Kuwano-Yoshida et al.*, 2010; *Ohfuchi et al.*, 2004] and the Coupled Ocean–Sea Ice Model for the Earth Simulator (OIFES) [*Komori et al.*, 2005, 2008]. The AFES is adapted from CCSR/NIES AGCM version 5.4.02 [*Numaguti et al.*, 1997] developed at Center of Climate System Research (CCSR) of University of Tokyo and National Institute for Environmental Studies (NIES). The OFIES is based on Modular Ocean Model version 3 (MOM 3) [*Pacanowski and Griffies*, 1999], developed at Geophysical Fluid Dynamic Laboratory (GFDL) and the sea ice model is based on that developed at International Arctic Research Center (IARC) of University of Alaska [*Zhang and Zhang*, 2001].

The integration analyzed in this study was run at a resolution of T119 (the triangle truncation at wave number 119, $\sim$1° in Gaussian grid) in the horizontal and 48 layers in the vertical for the atmosphere, and 0.5° x 0.5° horizontal and 54 vertical levels for the ocean [*Richter et al.*, 2010; *Taguchi et al.*, 2012]. Synoptic-scale disturbances in the atmosphere are well represented, but mesoscale eddies in the ocean cannot be resolved with the resolution of the model [*Taguchi et al.*, 2012]. To parameterize eddy effects on diffusive processes in the ocean, isopycnal mixing [*Redi*, 1982] and parameterized eddy-induced motions [*Gent and Mcwilliams*, 1990] are incorporated in OIFES. CFES has high resolution than most of the IPCC class (CMIP3) models, with no anthropogenic forcing and it achieves rather realistic stimulation of the Antarctic sea ice. The model was integrated for 120 years of which the last 100 years are analyzed. The trends are removed at each grid points.

2.2 Comparison between observed and modeled sea ice fields

2.2.1 Climatology

To examine the fidelity of the model, climatological structure of annual cycle and temporal mean structure of sea ice are compared between observation and model. As a representative variable, sea ice edge (SIE) is compared here. SIE is defined by the equatorward latitudinal position of 30% isopleth of SIC [*Yuan and Martinson*, 2000]. The annual cycle of the model SIE anomaly fits quite well with that of observation (Fig. 2.1a) especially in the autumn, winter and spring season. In summer there is positive bias in the model indicated by extensive SIE (around 2° from the observed SIE) which is lesser than most of the CMIP3 models [*Holland et al.*, 2005; *Landrum et al.*, 2012]. The internal variability of the climate system is assessed by computing the standard deviation of each month after removing the mean annual cycle from the observation and the model (Fig. 2.1b). The model overestimates the standard deviation all over the year, but the seasonal variability in the magnitude of standard deviation is relatively smaller throughout the year which is similar to that of observation.

The simulated climatological mean fields of annually averaged SIC agree fairly well between the observation(Fig. 2.2a and 2.2b). The agreement is good for Indian ocean and Ross sea regions, although the model overestimates the mean annual SIE in the Amundsen-Bellingshausen sea and Weddell sea region and underestimates in the Pacific ocean region (Fig. 2.2c). Nevertheless, the latitude of annually averaged

SIE of the model (62.6°S) corresponds to that of the observation with the zonally averaged difference of only 0.2 degree.

The climatological features from the observed SST is also well simulated by the model (Fig. 2.3). The mid-latitude SST frontal zone between 40°S and 50°S is also well represented in the model. Overall, the model represents observed mean patterns of SIE and SST fairly well.

2.2.2 Patterns of inter-annual variability

To study the characteristic variability of the Antarctic sea ice, statistical methods such as empirical orthogonal function (EOF) analysis, regression, correlation are applied for both observation and model results. The statistical significance of correlation coefficients is assessed using students t tests. The EOF analysis are based on temporal covariance matrix and are calculated for data anomaly first weighted by the square root of the cosine of latitude. The results are unweighted and then displayed. The analyzed model variable include SIC, SST and Geo-potential height (GPH) at 700 hPa. The data are detrended and its climatological mean removed and normalized by dividing the standard deviation before EOF analysis.

2.2.2.1 Observed sea ice and ocean

To examine the dominant pattern of observed sea ice variability, EOF analysis was applied for the period of 1979-2010. The spatial pattern of the first mode of the EOF of annual averaged satellite SIC exhibits opposite sign anomalies at Weddell sea and Antarctic peninsula sector (negative) and Amundsen sea and Ross sea sectors (pos-

itive) (Fig. 2.4). This pattern is similar to Antarctic Dipole [*Yuan and Martinson*, 2000; *Yuan*, 2004]. The spatial pattern have a variance of 15.2%. The oceanic parameter is represented by the SST. The SST pattern of first mode of EOF also shows a dipole structure with alternate anomalies at Weddell sea and Antarctic peninsula region and Amundsen sea and Ross sea sectors (Fig. 2.4b). The first mode of SST has a variance of 16.2%. The spatial patterns indicate a coupling between SIC and SST. Both SIC and SST have a dominant inter-annual time scale of 5-6 years which is comparable with previous studies (Fig. 2.5) [e.g., *Udagawa et al.*, 2009; *Landrum et al.*, 2012]. The high correlation (∼0.8 at zero lag) between SIC and SST further confirms a coupling between ice and ocean with increased SIC corresponding to decreased SST.

2.2.2.2 Model sea ice, ocean and atmosphere

In the model, the leading mode of SIC is a circumpolar pattern explaining 13% of variance (Fig. 2.6a) which is not revealed in the short satellite data. This mode has high decadal variability and will be discussed further in section 3.3. The spatial pattern of the second mode reveals a dipole between Belligshausen Sea and off Antarctic Peninsula, which corresponds to the ADP pattern detected in the satellite observation with an explained variance of 9.3% (Fig. 2.6b). The dominant time scale is 5-6 years, which is also comparable to the observation (Fig. 2.7).

The EOF analysis of SST reveals that the first mode is a circumpolar pattern which explains a variance of about 13% (will be discussed further in section 3.4) (Fig. 2.8a). The second mode with a variance of 9.6% has negative anomaly at the Ross sea and Amundsen sea sector and positive anomalies in the Drake Passage and Weddell Sea sector north of 60°S (Fig. 2.8b). This is similar to the first mode of the observed

SST. The power spectra reveals peaks between 5-6 years (Fig. 2.9). Similar to the observations, the model also shows a coupled relationship between second mode SIC and SST with good correlation (∼0.8 at zero lag) between them.

The spatial pattern of the leading mode of annual-mean geopotential height (Z) at 700 hPa is the circumpolar pattern with out-of-phase anomalies between the polar and sub-polar region (Fig. 2.10a), corresponding to that of SAM [*Thompson and Wallace*, 2000] which explains about 31% variance (more discussion in section 3.4). The second mode (Fig. 2.10b) has a dipole structure of alternating anomalies in the Pacific sector, which corresponds to the PSA pattern [*Karoly*, 1989; *Udagawa et al.*, 2009]. Its time score has spectral peaks between 3-6 years (Fig. 2.11).

Thus the model could simulate the mean climatological fields and inter-annual variability in SIC and SST very well. It also captures the observed spatial patterns in SIC and SST in the inter-annual time scale reasonably well. It also simulate the leading atmospheric modes really well. This similarity to observations suggest that the variability and its driving forces are well simulated. Moreover, the model has very narrow difference in magnitude of inter-annual variability in SIE from one season to other (Fig. 2.1b), justifying the use annual mean in the analysis. Hence the model can be used to study the longer term variability in the Antarctic sea ice.

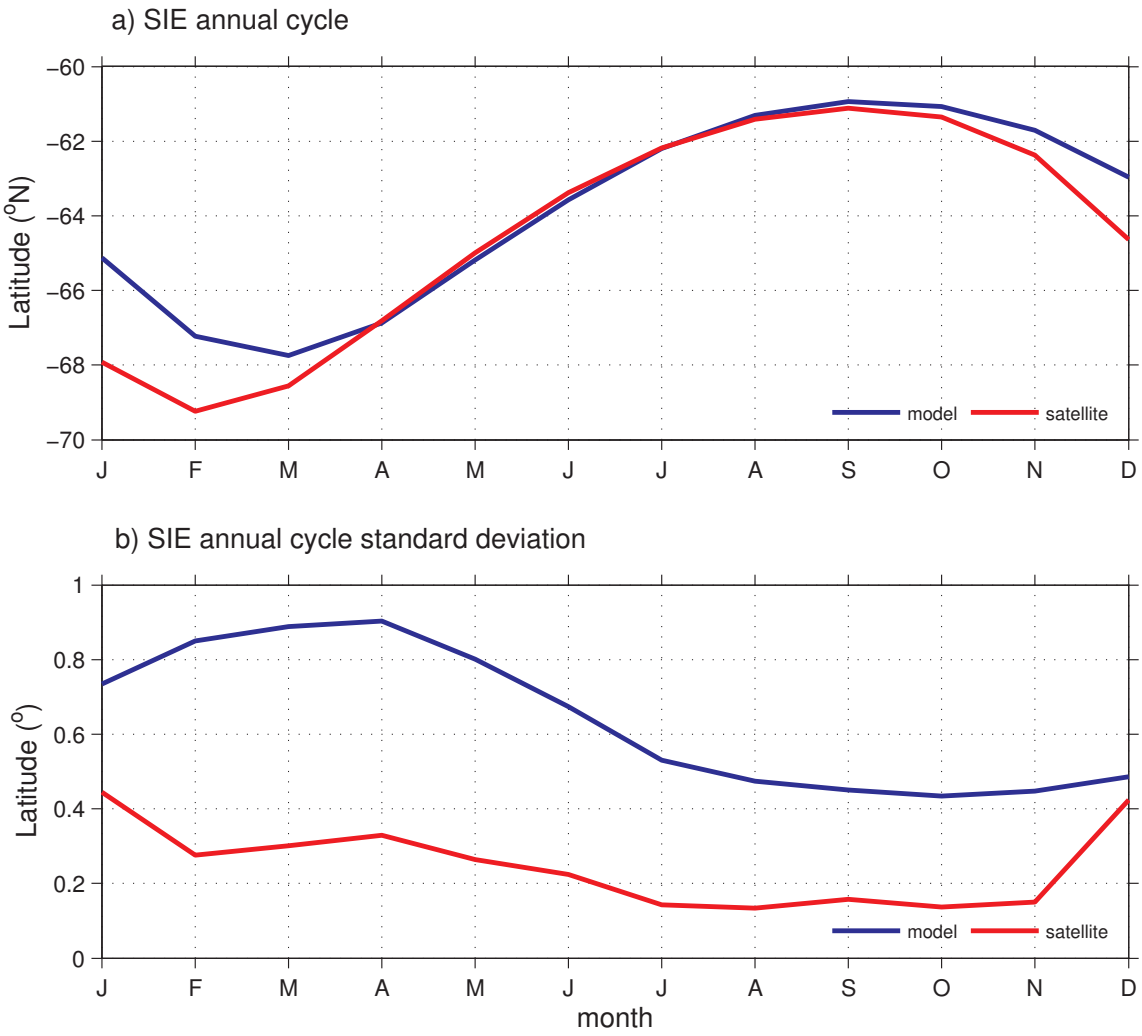

Figure 2.1: a) The annual cycle of sea ice edge from satellite (1979-2010) and model (21-120) and b) the standard deviation of the sea ice edge for each month. The red line indicates the satellite and the blue line the model.

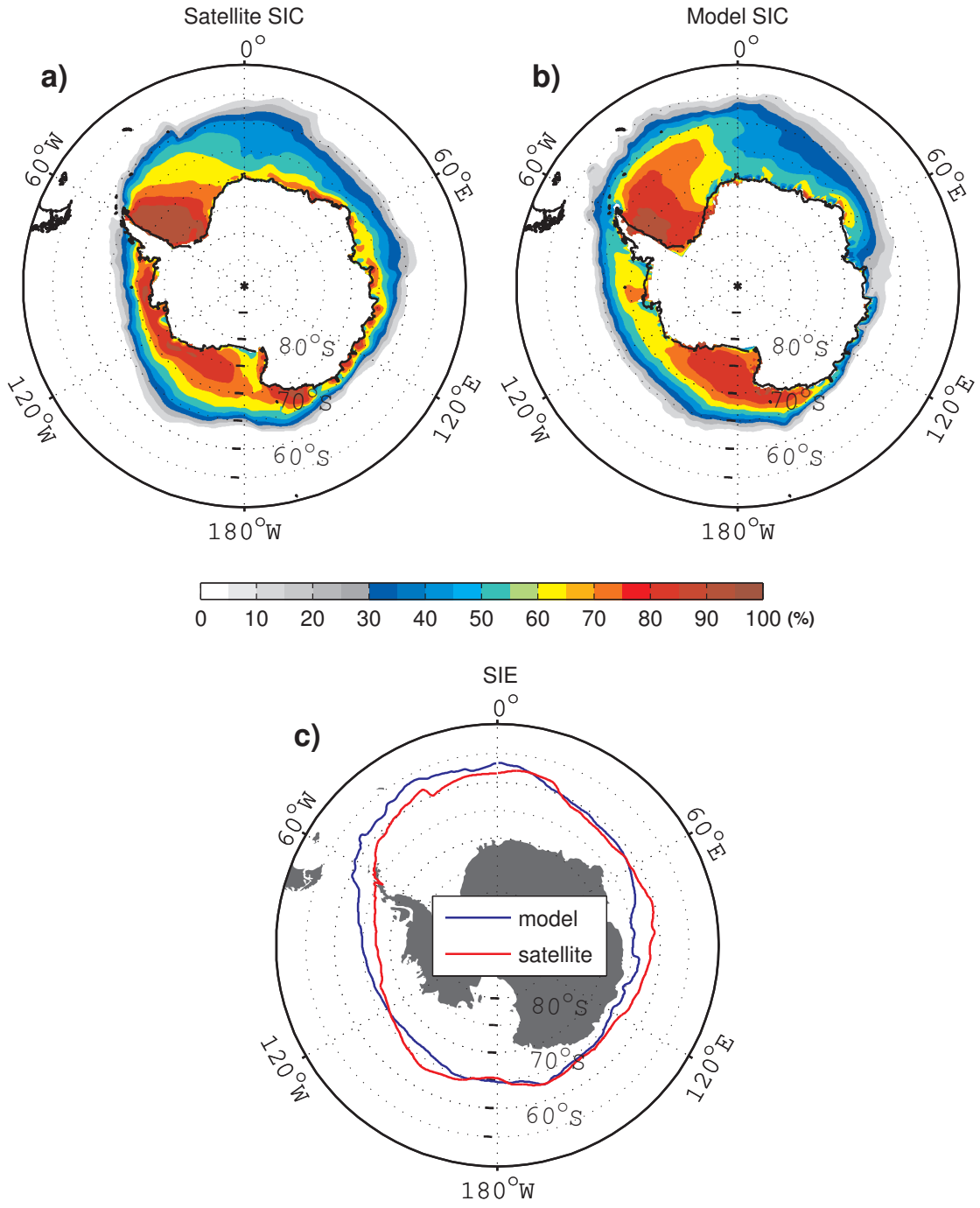

Figure 2.2: The annual climatology of sea ice concentration [%] from the a) satellite observation data and b) model. c) Sea ice edge of annual mean sea ice concentration from the satellite data and model. The red line indicates the satellite and the blue line the model.

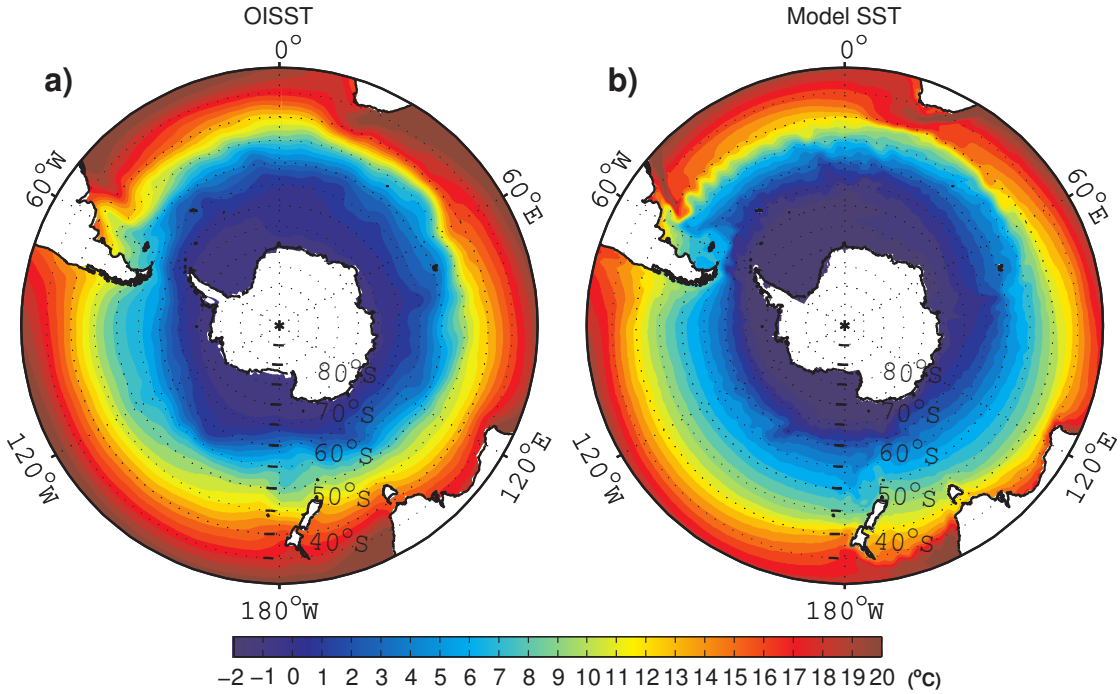

Figure 2.3: Spatial distribution of annual climatological mean of sea surface temperature in °C from a) observation (1982-2010) and b) model (21-120).

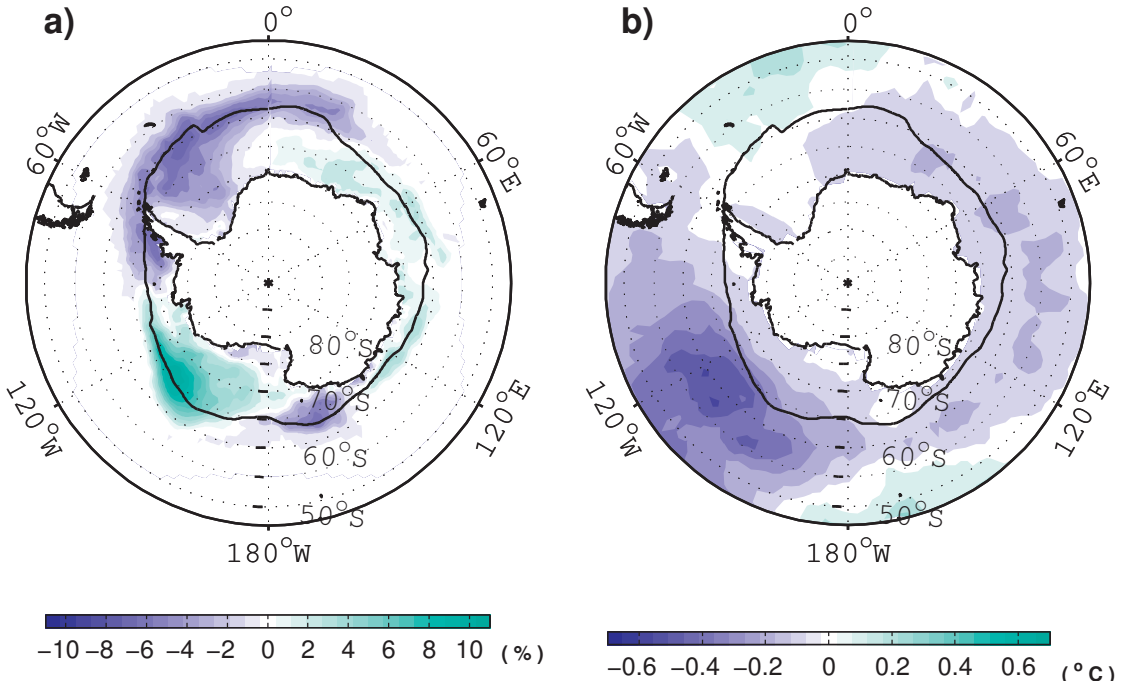

Figure 2.4: Spatial pattern of leading mode of annual mean a) sea ice concentration anomalies [15.2% variance], b)sea surface temperature anomalies [16.2% variance] from the observation data. The EOFs have been scaled by 1 standard deviation of the corresponding principal component time series to show the dimensional standard deviation at each grid point in the EOF. The black line show the location of annual mean sea ice edge from satellite.

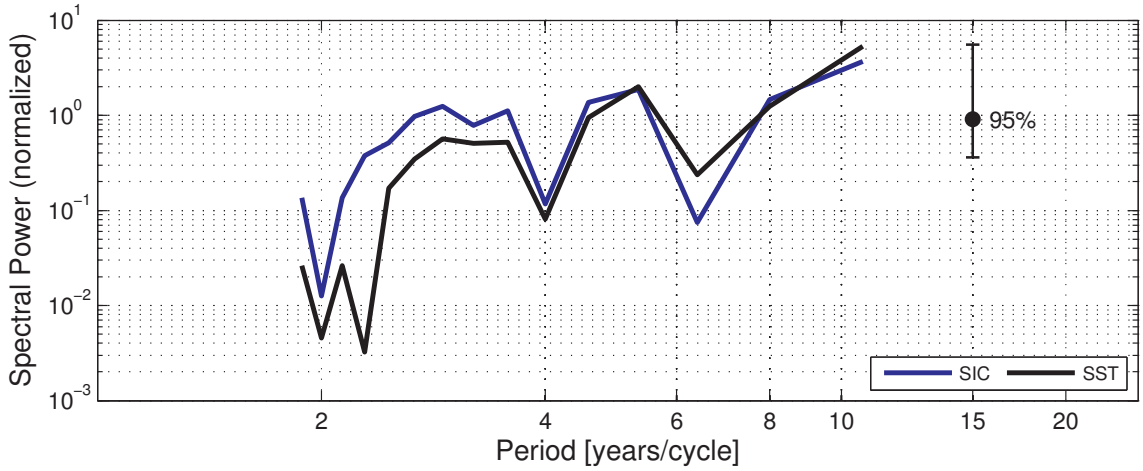

Figure 2.5: Power spectrum of the principal component time series of the first mode of sea ice concentration (blue) and sea surface temperature (black) from observation.

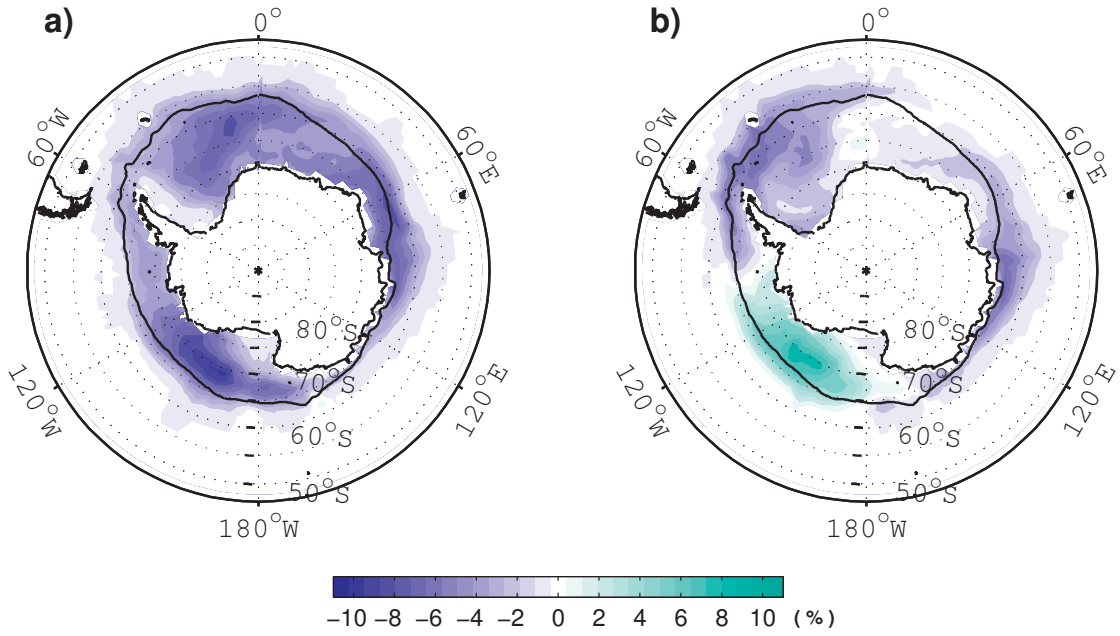

Figure 2.6: Spatial pattern of a) first mode [12.9% variance] and b) second mode [9.3% variance] of EOF of annual mean sea ice concentration anomalies from model. The EOFs have been scaled by 1 standard deviation of the corresponding principal component time series to show the dimensional standard deviation at each grid point in the EOF. The black line show the location of annual mean sea ice edge of the model.

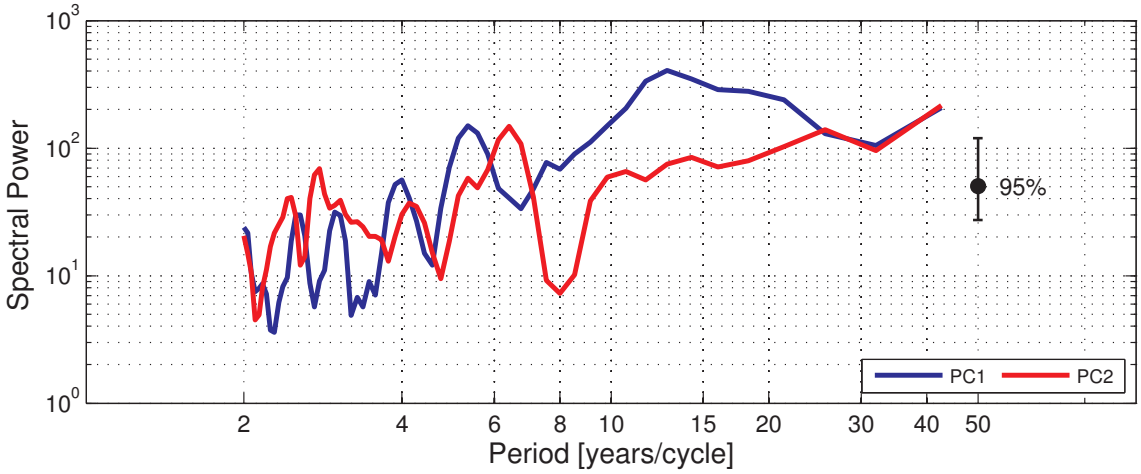

Figure 2.7: Power spectrum of the principal component time series of the first mode (blue) and second mode (red) of sea ice concentration from the model.

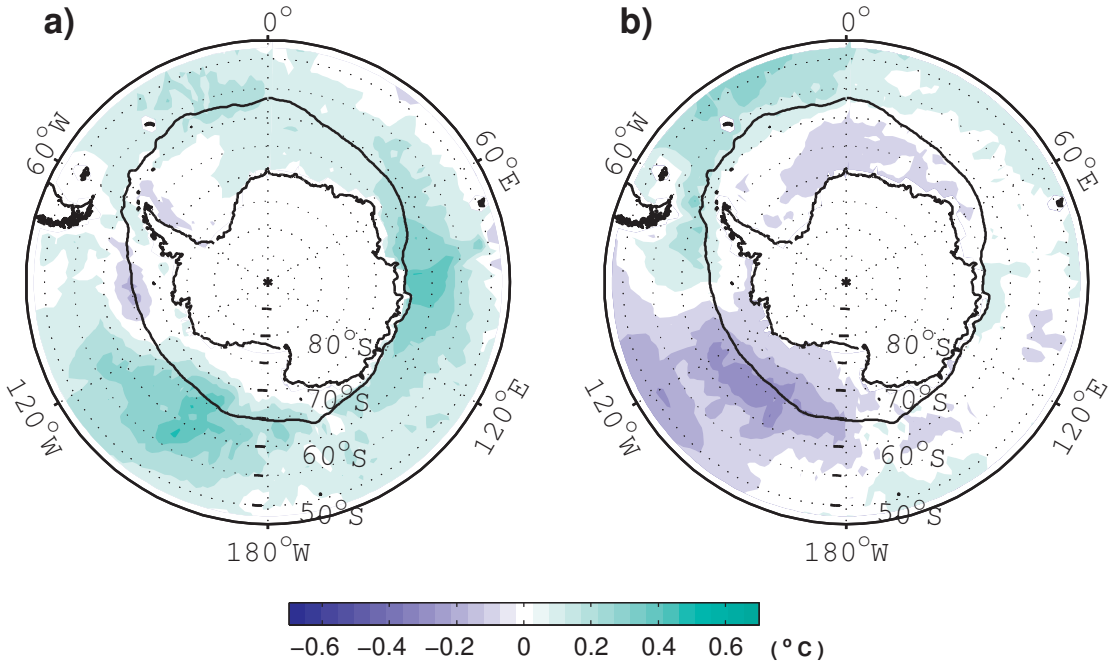

Figure 2.8: Spatial pattern of a) first mode [13.3% variance] and b) second mode [9.6% variance] of EOF of annual mean sea surface temperature anomalies from model. The EOFs have been scaled by 1 standard deviation of the corresponding principal component time series to show the dimensional standard deviation at each grid point in the EOF. The black line show the location of annual mean sea ice edge of the model.

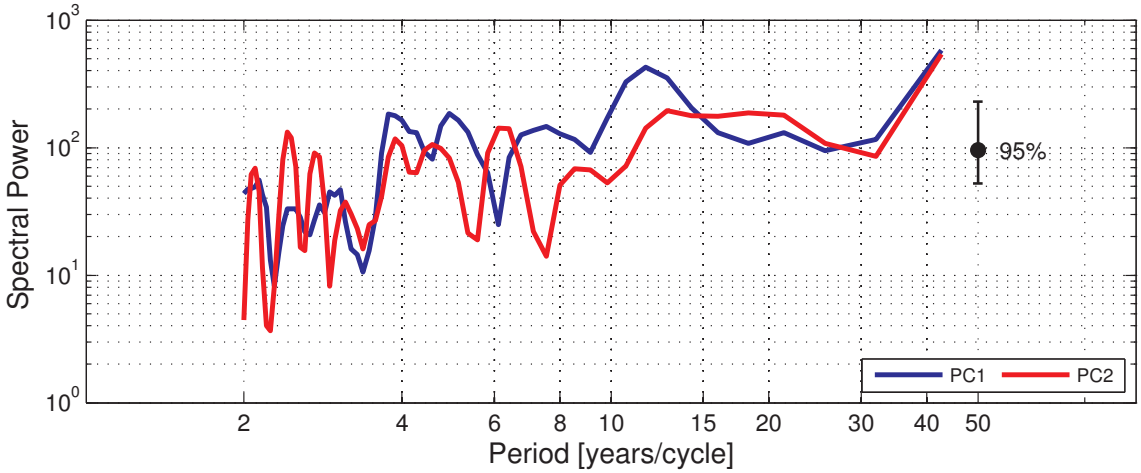

Figure 2.9: Power spectrum of the principal component time series of the first mode (blue) and second mode (red) of sea surface temperature from the model.

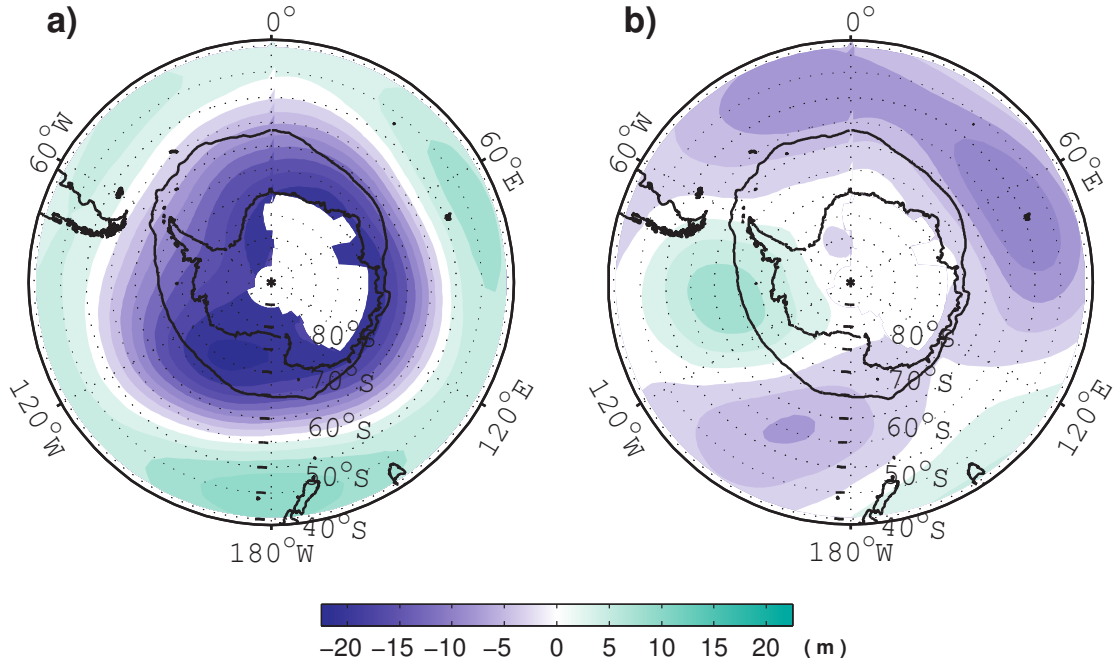

Figure 2.10: Spatial pattern of a) first mode [31.3% variance] and b) second mode [11.61% variance] of EOF of annual mean geo-potential height anomalies at 700 hPa from model. The EOFs have been scaled by 1 standard deviation of the corresponding principal component time series to show the dimensional standard deviation at each grid point in the EOF. The black line show the location of annual mean sea ice edge of the model.

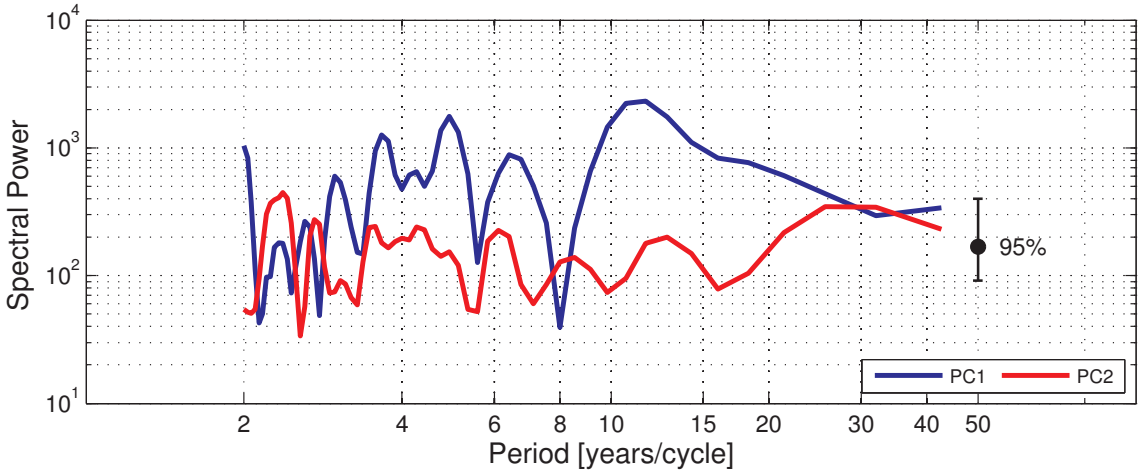

Figure 2.11: Power spectrum of the principal component time series of the first mode (blue) and second mode (red) of geo-potential height at 700 hPa from the model.

Chapter 3

Pattern of decadal variability of Antarctic sea ice

3.1 Overview

As presented in the EOF analysis of the model results, annular variabilities are dominant in sea ice and ocean surface temperature on the decadal time scale. In this chapter we focus on the behavior of the decadal variability of the Antarctic sea ice. Observational results are reexamined from the point of view of the annular mode structure. An EOF analysis is performed to characterize the spatial and temporal structure of variabilities derived from the model. The spatial coverage of the SIC for EOF analysis was the entire area of Antarctic sea ice (approx 40°S - 90°S latitude band) and from 20°S - 90°S latitude band for SST and GPH, so that leading oceanic patterns including frontal zones beyond SIE and extratropic atmospheric circulation patterns could be identified .The spatial patterns associated with each EOF are rep-

resented by the dimensional standard deviation at each grid point in the EOF. That is the EOF's are scaled by unit standard deviation of the PC time score resulting in a map with original units of the variable. We focus on the annual average of the variables. The temporal relationships among the SIC, SST and GPH patterns are then investigated.

3.2 Decadal variabilities in observed sea ice, SST and SAM

To examine the decadal variability of circumpolar SIE pattern, zonally averaged SIE is examined from the 32-year satellite observation record (Fig. 3.1a). The low-pass filtered (7-yr fft) circumpolar SIE shows the increasing trend with negative anomalies from late-1980s to early 1990s and early 2000s and positive anomalies in late 1990s. Taking zero-crossing points after subtracting the trend, the SIE exhibits decadal variability with the period of 11-16 years.

To examine the coupling between the sea ice and ocean, SST anomaly, averaged for the 5 degree bin from the climatological SIE, are derived and averaged zonally. The SST shows a decreasing trend with a prominent temporal fluctuation with positive anomalies in early 1990s and 2000s and negative in late 1990s (Fig. 3.1b). After taking the low-pass and subtracting the trend, the period of 11-13 years is estimated by zero-crossing. The correlation coefficient between the SIE and SST was -0.68 and -0.51 at 1 and 0 year lag in SST, respectively. This negative correlation indicates that high (low) SST corresponds to retreat (expanded) SIE, although it is not highly

statistically significant due to the low degree of freedom.

The SAM index, which represents the circumpolar atmospheric field, shows a decadal period of 11-13 years with the general increasing trend (Fig. 3.1c). The correlation between SIE and SAM is positive (0.78 and 0.63 at 1 and 0 year lag in SAM, respectively), although the correlation coefficients are not statistically significant. To summarize, there is a long-term Antarctic SIE increasing trend, associated with the long-term cooling surface ocean and increasing SAM trends on the decadal time scale from about 30-year observation records, although statistical significance is low presumably due to a short observation period.

3.3 Dominant mode of decadal sea ice variability

To examine the modes of simulated sea ice variability on the decadal or longer time scales, spatial patterns and temporal characteristics are investigated. The leading mode of SIC is a quasi-circumpolar pattern explaining ∼13% of variance (Fig. 3.2a). The pattern is almost annular, with prominent intensification located at the eastern end of the Weddell Gyre and the eastern Ross sea sector. The spectrum analysis reveals a broad peak at time scales of 12-17 years (Fig. 3.3), whereas the second mode (Fig. 2.7) has no significant peak in the decadal time scale. Hence the model's leading mode is the quasi-circumpolar pattern on the decadal time scale, which was not revealed as a higher mode in the shorter-satellite records of SIC (Fig. 2.4 and Fig. 2.5).

3.4 Dominant oceanic and atmospheric patterns and their relationship with sea ice

To explain the dynamics of the dominant mode of sea ice variability, EOFs of the model atmospheric and oceanic variables are examined.

The spatial pattern of the leading mode of annual mean GPH is the circumpolar pattern with out-of-phase anomalies between the polar and sub-polar region (Fig. 3.2b), corresponding to that of SAM [*Thompson and Wallace*, 2000]. This mode explains about 31%, which is also comparable to the SAM revealed in various reanalysis studies [*Thompson and Wallace*, 2000; *Yuan and Li*, 2008]. Its time score has a prominent spectral peak at around 11-12 years with additional inter-annual peaks at 3-5 years (Fig. 3.3).

The EOF analysis of SST reveals that the first mode is a circumpolar pattern, which explains about 14%, with high variability in the Indian ocean and Ross sea sector (Fig. 3.2c). This pattern is similar to the first mode in the SIC anomaly. The spectral structure of time score has peaks on around 11-13 years (Fig. 3.3). Hence the modeled leading mode of SIC, GPH, and SST are the quasi-circumpolar patterns which have large amplitudes on decadal time scales.

The covariability among the quasi-circumpolar modes of SIC, GPH and SST is examined by lagged correlation analysis of the low-passed (5-year running average) time scores (Fig. 3.4). The quasi-circumpolar SIC has a high correlation (~ 0.69) with the circumpolar SST at zero lag at significance level of 95%, indicating that less (more) sea ice corresponds to the warmer (cooler) temperature around the SIE. The quasi-

circumpolar SIC shows a correlation of ∼-0.35 with GPH at zero lag, indicating less (more) sea ice corresponding to negative (positive) SAM, although it is not statistically significant. SST and GPH circumpolar modes show a high negative correlation (∼-0.57) at zero lag; the cooler (warmer) SST around the SIE corresponds to the positive (negative) SAM. Hence the lagged correlation between the principal component time series of the circumpolar modes of SIC, GPH and SST shows qualitatively the same relationship that were revealed in the observation records, suggesting the presence of the coupled variability among those variables. The higher correlation between the oceanic and sea ice variability than that of the atmosphere and sea ice suggests that the quasi-circumpolar SIC variability is mainly driven by oceanic variability on this decadal time period.

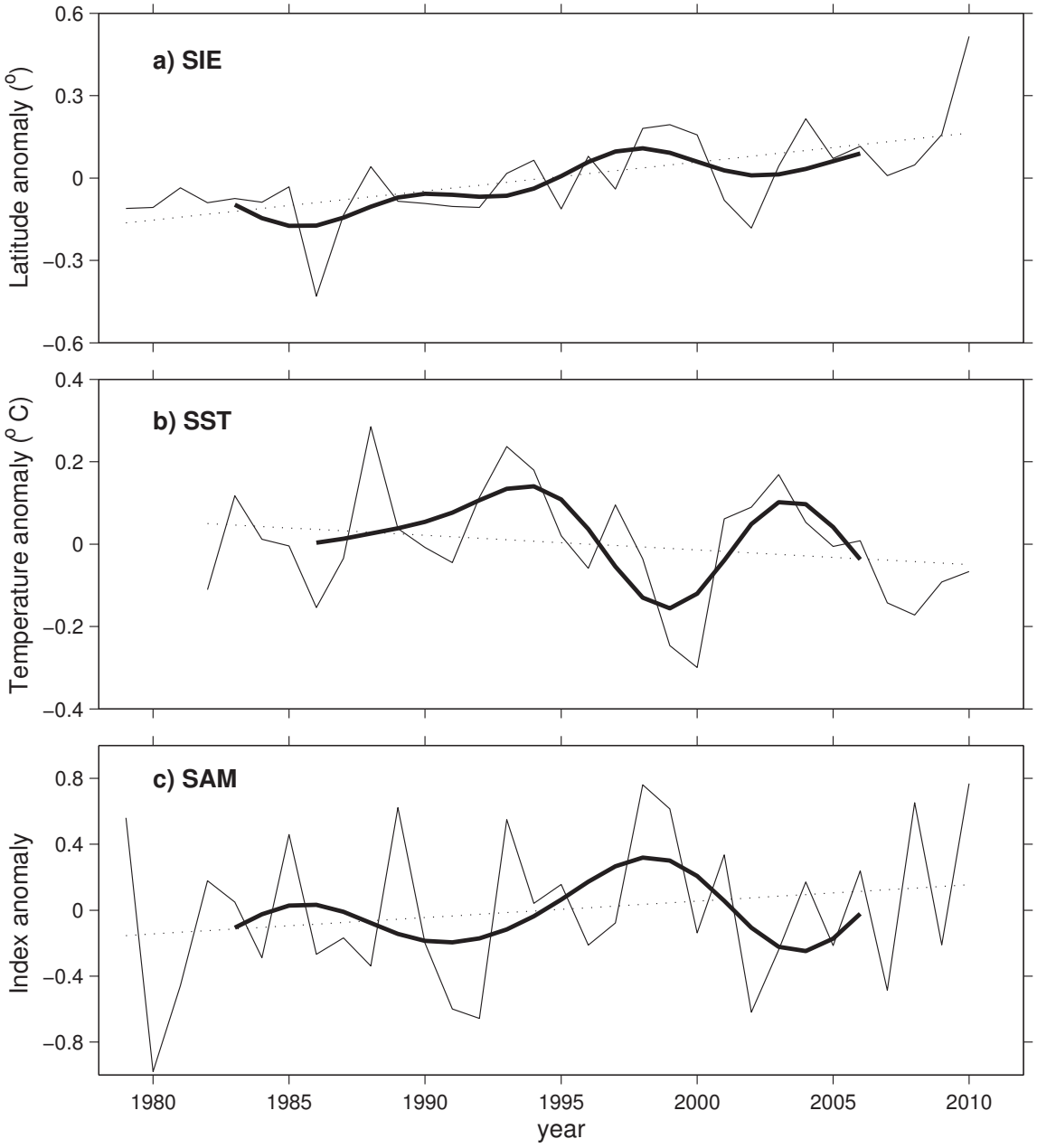

Figure 3.1: a) Observed circumpolar averaged annual sea ice edge (SIE) anomaly time series (1979-2010) b) observed annual circumpolar sea surface temperature [northward 5° latitude band from the SIE] anomaly time series (1982-2010) and c) annual SAM index (1979-2010) from Climate Prediction Center. The bold line represents a low passed (7 years) time series using a fft filter.

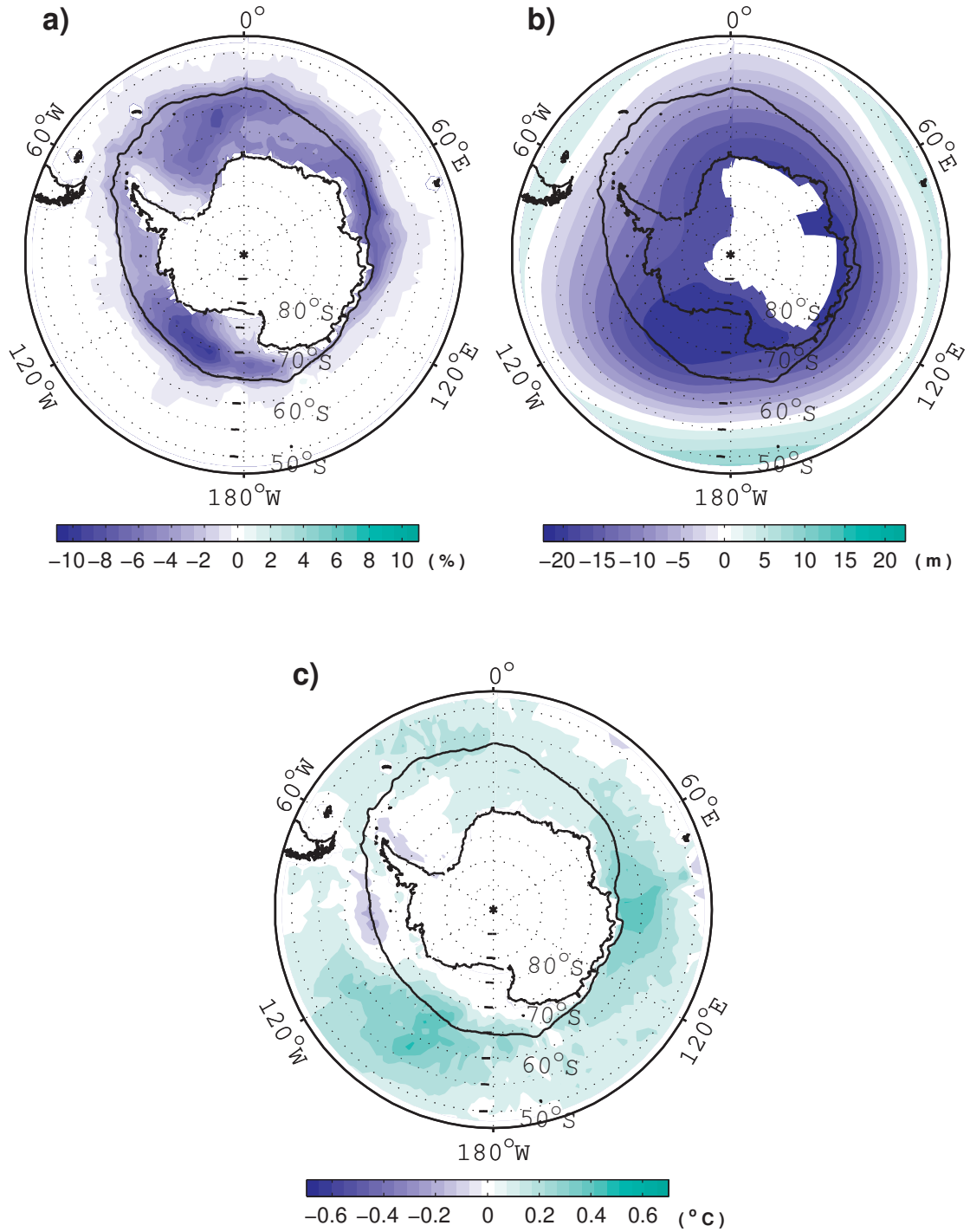

Figure 3.2: Spatial patterns of leading mode of annual mean a) sea ice concentration anomalies [12.9% variance] b) geo-potential height anomalies at 700 hPa [31.3% variance] and c) sea surface temperature [13.3% variance] anomalies from model. The EOFs have been scaled by 1 standard deviation of the corresponding principal component time series to show the dimensional standard deviation at each grid point in the EOF. The black line indicates the mean sea ice edge of the model.

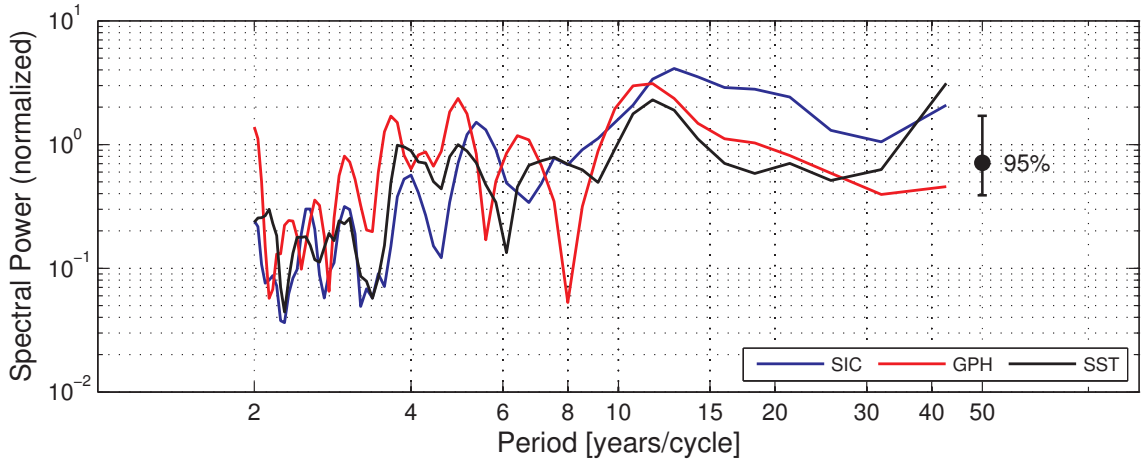

Figure 3.3: Power spectrum of the principal component time series of first mode of sea ice concentration (blue line), geo-potential height at 700 hPa (red line) and sea surface temperature (black line).

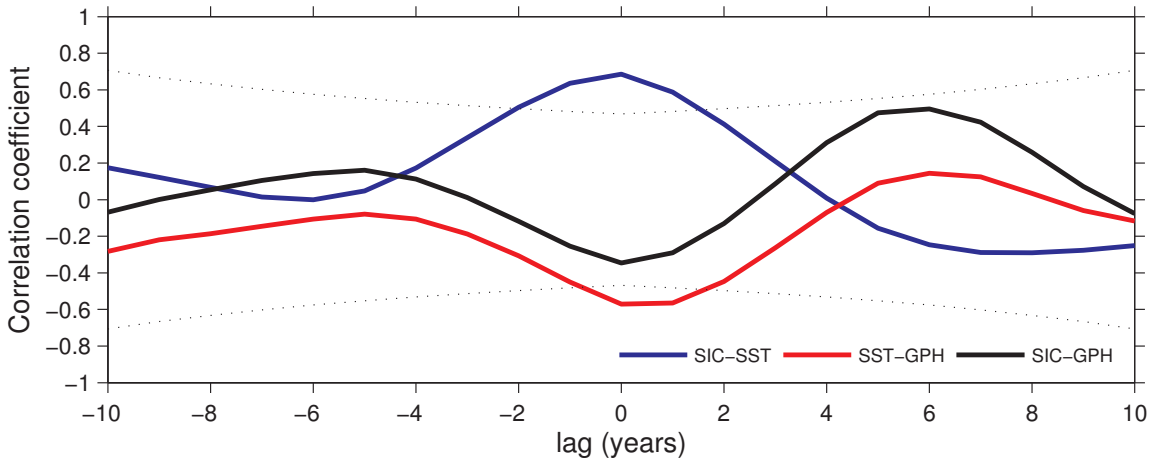

Figure 3.4: Lagged correlation between the 5 year running averaged principal component time series of the first modes of sea ice concentration and sea surface temperature (blue line) [r = 0.69 at 0 lag], sea surface temperature and geo-potential height at 700 hPa (red line) [r = -0.57 at 0 lag] and sea ice concentration and geo-potential height (black) [r = -0.35 at 0 lag]. The dotted line indicates the 95% confidence limit.

Chapter 4

Mechanism of decadal variability of Antarctic sea ice

4.1 Overview

Ocean have a longer residence time of anomaly compared to atmosphere. As we had observed a higher coupling between ocean and sea ice compared to sea ice and atmosphere, we will examine into the ocean interior. In the Southern Ocean warm circumpolar deep water (CDW) is underneath the cold surface water and hence heat source is in subsurface. In this chapter we analyze the variability in the mixed layer temperature (MLT), which should be consistent with SST, and the temperature below. The annual mean model mixed layer depth (MLD) (Fig. 4.1) is qualitatively similar but slightly underestimated as compared to that has been observed by *Dong et al.* [2007] using Argo profile data. The annual MLT is the potential temperature averaged over the annual MLD. The relationship between the MLT and temperature below are

examined, considering the upwelling velocity which is closely related to atmospheric forcing.

4.2 Decadal variability of ocean mixed layer and sub-surface layer

As has been observed in section 3.4 that the model decadal SAM shows a coupled linear relationship with the decadal circumpolar SST. The response of long-term MLT to SAM is also quasi-circumpolar pattern similar to the leading mode in SST (Fig. 4.2). To further investigate the temporal variability in the long-term circumpolar MLT we look at the time-latitude graph using the zonally averaged values of MLT anomaly(Fig. 4.3). Prior to zonally averaging the data is filtered using a running averaged band pass filter (7-21 years) so that the data mainly contains the signals of decadal variability. Alternate patterns of high and low anomalies with long-term variability could be observed. They have a decadal periodicity of 12-14 years. Each opposite signed anomalies are slightly propagating equatorward. The propagation speed (0.45 km/day) roughly corresponds to the mean meridional ocean surface velocity (v) (0.59 km/day) between 60°S-65°S. This propagation of anomalies from the vicinity of Antarctic continent and towards the equator hints at a mechanism associated with Ekman transport and upwelling.

To investigate further the reasons causing the alternating changes in the MLT we look at the vertical oceanic advection patterns where the source of propagating anomalies is located. Figures. 4.4a and 4.4b shows the leading modes of annual mean

oceanic vertical velocities (w) at depths of 100 m (EOF1) corresponding to the surface layer and at 450 m (EOF2) which is associated with layer of temperature maximum around the polar region in the model. EOF1 of w at 450 m is not shown as the mode shows a very low frequency variability as it is not relevant to present decadal time scale analysis. The spatial patterns shows a circumpolar pattern representing upwelling at the vicinity around the Antarctic continent between 70°S-55°S and downwelling to north of 55°S. The variance observed is 4.9% and 3.5% which is very less. Nevertheless, we get an idea of dynamic of the ocean. The high positive correlation [r = 0.86 at 0 lag for 100 m and r = 0.61 at 0 lag for 450 m] (Fig. 4.5) of the 5 year running average time series with SAM further confirms the relationship that at a longer time scale high positive SAM causes upwelling around the Antarctic continent associated with the northward Ekman transport as a result of SAM wind anomalies.

We look at the vertical temperature anomaly distribution at 65°S (corresponding to the highest upwelling area). The data is band passed (7-21 years) before taking the zonal average. We could observe anomalous temporal signals of opposite signs at periodic intervals between the mixed layer(50 m) and subsurface depth (below 100 m). The subsurface water below 200 m is characterized by the upper boundary of the CDW with salinity 34.65-34.68 psu and temperature 0.5-1.5 °C between 65°S-60°S. It is likely that the anomalies advect upwards indicating an upwelling signal (Fig. 4.6a). Estimating the time series data from depths of 400-500 m which represents the depth level of temperature maximum and 50 m which represents the mixed layer and by comparing both time series, it could be observed that the signals at the subsurface are in phase to the surface signal (Fig. 4.6b). In other words, the mixed layer has

similar temperature anomaly compared to the temperature at subsurface depths. The time scale of upwelling of the subsurface water to come to the surface, calculated from the low pass filtered circumpolar mean vertical velocity ($\bar{w} = 24.8$ m/yr) between 400-500 m depth, is 14-18 years. The time scale agrees well with the frequencies of the coupled decadal variabilities.

To summarize the decadal upwelling of the warm subsurface water around the Antarctic continent due to long term increase in SAM increasing the SST, decreases the sea ice, induces the decadal variability in the sea ice. The upwelling change is strongly connected to the atmospheric wind change. Linkage between these mechanism will be further elaborated in chapter 5.

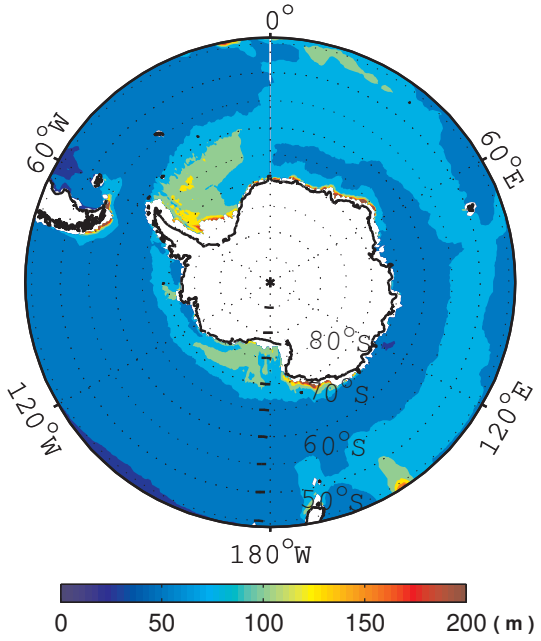

Figure 4.1: Spatial distribution of annual mean mixed layer depth in the Antarctic region.

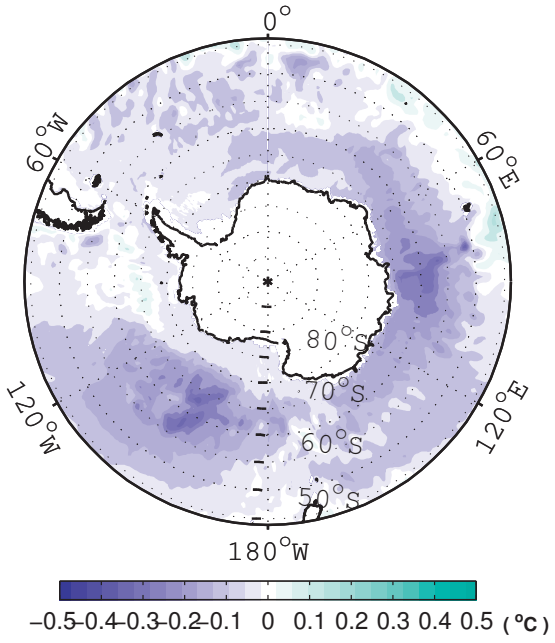

Figure 4.2: Regression of the mixed layer temperature (5 year running averaged) onto the SAM index (5 year running averaged).

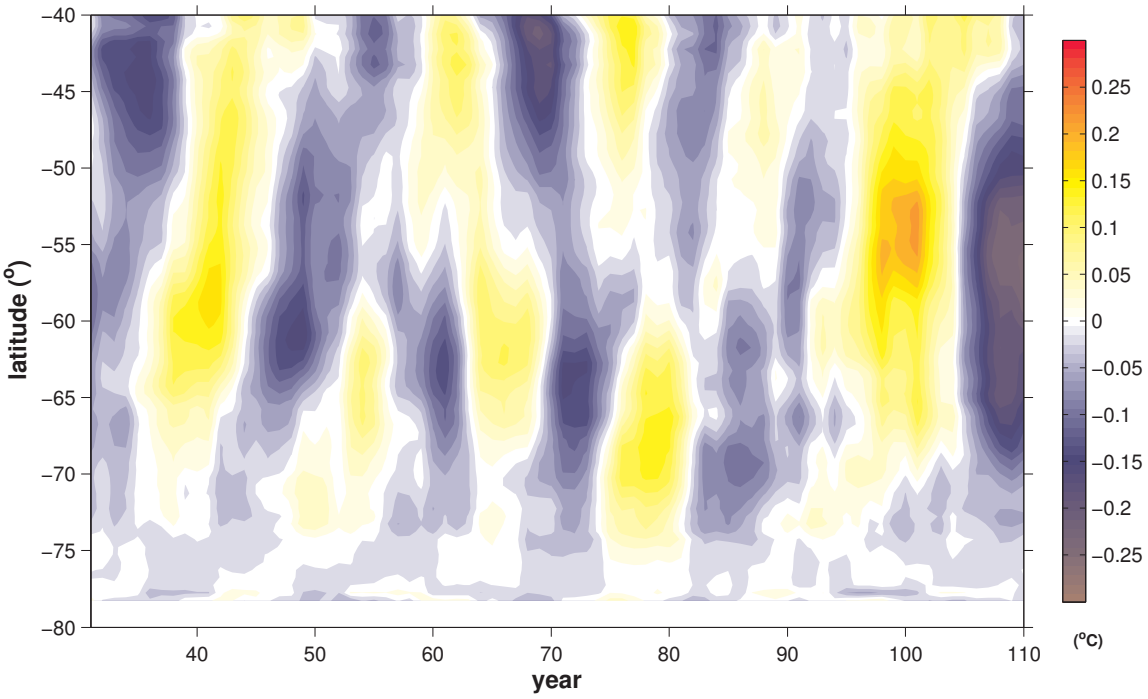

Figure 4.3: Latitude-time diagram of zonal mean of mixed layer temperature. The data has been band passed between 7 to 21 years using a running average filter to extract the decadal signal.

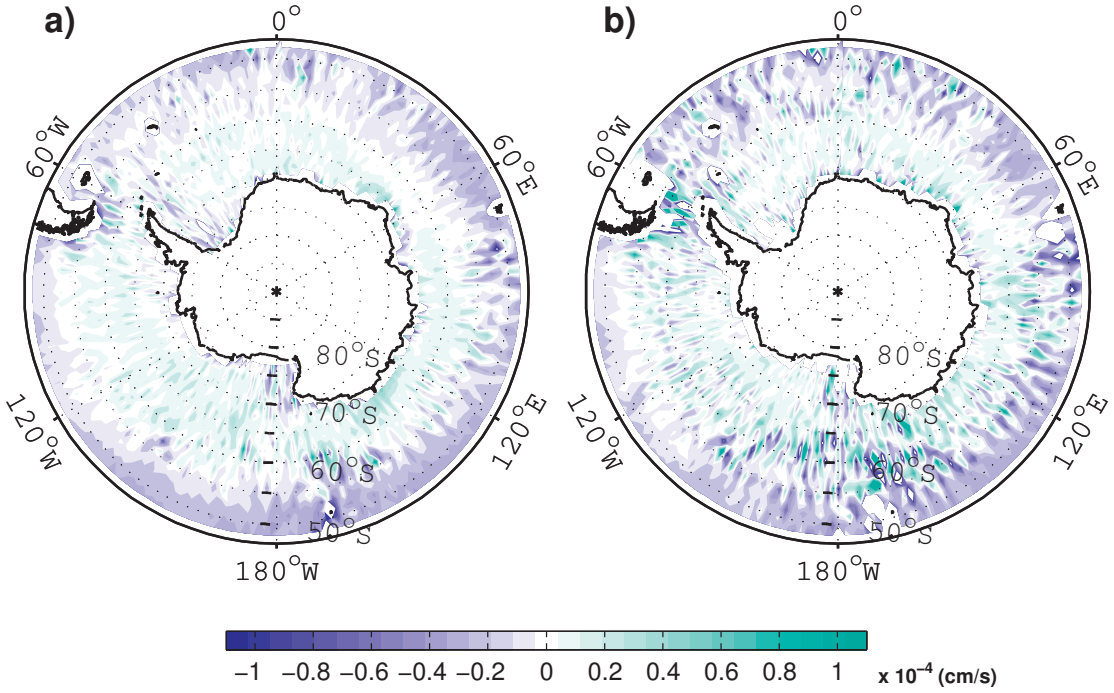

Figure 4.4: Spatial patterns of leading mode of annual mean a) oceanic vertical velocity (w) anomalies [4.9% variance] at 100 m (EOF1) and b) at 450 m [3.5% variance] (EOF2) from the model. The EOFs have been scaled by 1 standard deviation of the corresponding principal component time series to show the dimensional standard deviation at each grid point in the EOF.

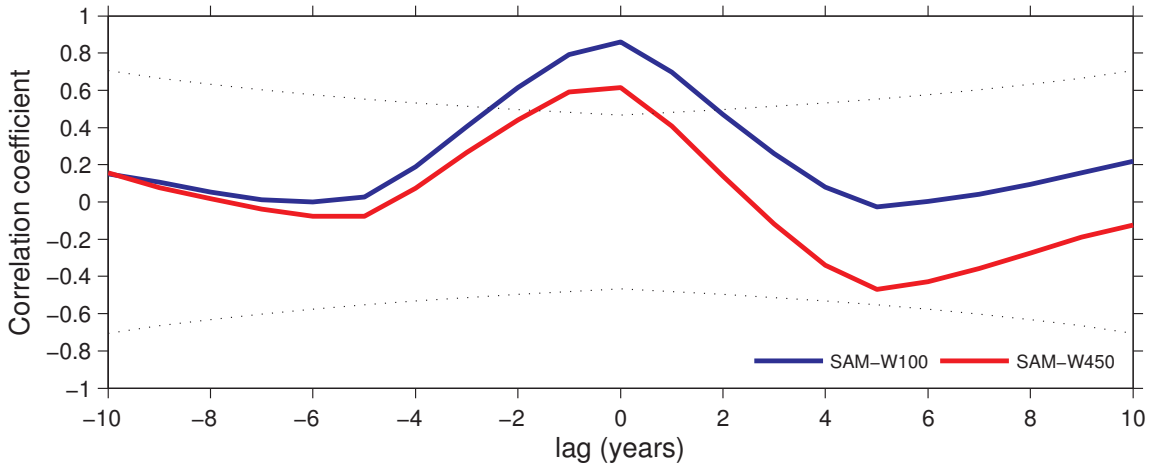

Figure 4.5: Lagged correlation between the principal component time series (5 year running averaged) of the first mode (PC1) of geo-potential height with PC1 of vertical velocity (w) at 100 m (blue line)[r = 0.86 at 0 lag] and with PC2 of w at 450 m (red line)[r = 0.61 at 0 lag]. The dotted line indicates the 95% confidence limit.

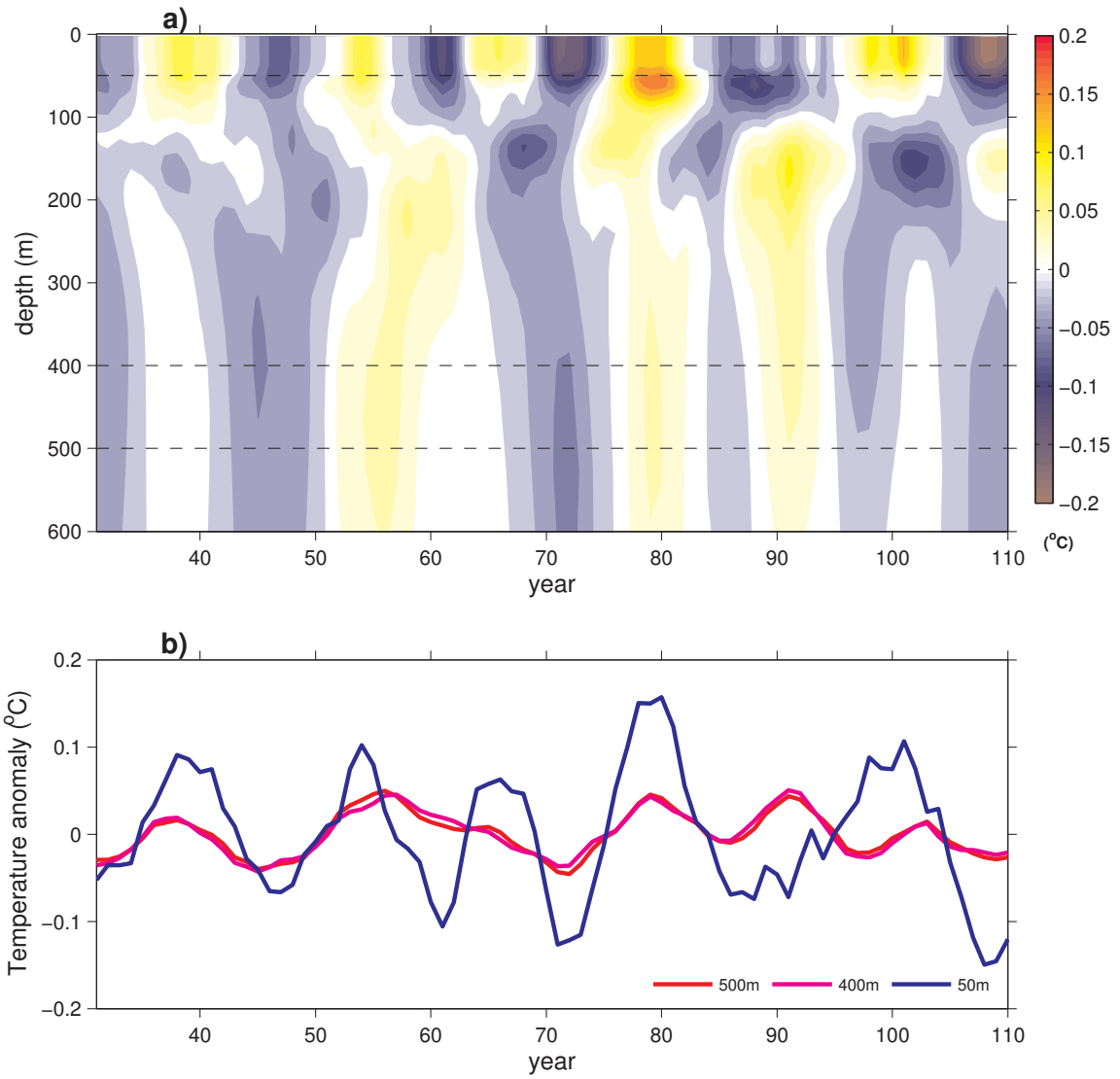

Figure 4.6: a) Temporal distribution of vertical oceanic temperature anomaly (^{o}C) at 65^{o}S. b) The time series of temperature anomaly at the depths 500 m (red line), 400 m (magenta line) and 50 m (blue line). The corresponding depths in b) are indicted by the dashed black lines in a). The temperature is zonally averaged and band passed (7-21 years running average filter).

Chapter 5

Discussion

We showed the model fidelity on the decadal variability of sea ice. Here we will assess the model performance with similar modeling outcomes. We obtained the coupled annual variability of sea ice-ocean-atmosphere on the decadal time scale from both observations and model. The dominance of this mode is discussed statistically here. Finally we will investigate the mechanism of this coupled decadal variability.

The analysis of the output from CFES and observations shows that the model has good reproducibility of the climatological mean condition in SST and SIC parameters. Recent model studies [*Turner et al.*, 2013; *Zunz et al.*, 2013] using CMIP5 models showed that most of the models overestimated the variability of the sea ice extent in winter and the variability in some models vary significantly from one season to other compare to the satellite observation. Some model [*Sen Gupta and England*, 2006; *Capotondi et al.*, 2006] revealed PSA as two year period as opposed to 3-7 year period in the observations. Further some of the IPCC-AR4 models, were unable to reproduce the observed inter-annual variability patterns in the Antarctic sea ice [*Holland et al.*,

2005]. CFES could represent well the observed inter-annual ADP pattern in SIC and SST. It also simulates well the atmospheric PSA (Fig. 2.10b) circulation pattern and its time scale and shows a significant correlation with SST (r = ∼0.6 at 0 lag) and SIC (r = ∼0.3 at 0 lag) on an inter-annual time scale. The fact that the model reproduces PSA mode at the same period lends further support for the model fidelity on the longer-time scale variability.

The observational records of sea ice have revealed a circumpolar variability of SIE on decadal time scale. SST observations and SAM record also showed variation on similar time scales with warm (cool) anomaly corresponding to retreat (extension) of SIE at negative (positive) SAM. The presence and periodicity of the decadal variabilities in SST and SAM are consistent with those described by *Yuan and Yonekura* [2011], who estimated from different observation and reanalysis data. These relationships are also confirmed from our model study. The model and observation show a good quantitative agreement. The correlation coefficients between the circumpolar SIE and SST anomalies are similar between model and observation (∼0.6-0.7). The magnitudes of the variabilities compared reasonably well quantitatively between the observation and model. When the circumpolar average anomalies at SIE are calculated as in the same manner with the observation (Fig. 3.1), the model circumpolar SST decrease (increase) of 1°C corresponds to 1.4 degree extension (retreat) of circumpolar SIE latitude towards north (south) from the linear regression, while the SST anomaly of 1°C corresponds to 0.4 degree in latitude in the observation. Although the model response is slightly larger than that of the observation, the comparison agrees well given the fact that the model does not aim to reproduce the same period and

uncertainty caused by different record lengths used as we discuss below.

The first EOF mode from observed satellite sea ice is a dipole pattern, not annular (Fig. 2.4a), whereas the model leading mode is an annular pattern (Fig. 3.2a). This is probably due to the shorter record length (around 30 years) of satellite sea ice data and also depends on the position of the time series segment in a long period oscillation. An EOF analysis of different time series segment (30 years) of the model data reveals that there is only 50% possibility of occurrence of annular mode as the leading mode in a shorter length time series data (Fig. 5.1). For the other half representations the patterns resemble to the dipole. In other words, 30 years of sea ice data is statistically insufficient for the projection of annular leading mode.

The decadal variability in SST sets the time scale of decadal variability in the sea ice. The upwelling of subsurface warm water increases the surface temperature thereby reducing the sea ice. Here the mixed layer depth is considered at 50 m and the subsurface depth at a layer 400-500 m corresponding to temperature maximum. The time period of upwelling is 14-18 years. This time scale is similar to the spectral peak observed for the first EOF of SST. The upwelling velocity increases as the depth decreases as there is more atmospheric influence. The period of upwelling is around 14-16 year for a water column at 300 m and 11-13 years at 200 m. Overall the time scale of consistently decadal at different subsurface depths. Given this time scale, we illustrate a possible interplay of feedback mechanisms that sets the time scale of this coupled variability in the climate system (Fig. 5.2). Cooler SST in the south during positive SAM, and hence stronger temperature gradient, enhances the atmospheric cyclogenesis and intensifies the near surface westerlies [*Marshall and Connolley*, 2006],

leading SAM towards a more positive state. The cooler SST and stronger SAM contributes the equator-ward expansion of SIE. This is a positive feedback. On the other hand, stronger westerly enhances upwelling around the vicinity of the Antarctic continent and brings warmer subsurface water to the surface [*Lefebvre et al.*, 2004; *Lefebvre and Goosse*, 2005]. This warmer SST then sets up a negative feedback, weakening the cyclogensis and SAM and causing a pole-ward retreat of SIE. The switching of the coupled feedback mechanisms, which is regulated by the time scale of upwelling, could be the driving mechanism causing the circumpolar variability on a decadal time scale.

Although some models [e.g., *Sen Gupta and England*, 2006] found little evidence on the role of upwelling in SST changes around Antarctic continent, our results show that upwelling around the Antarctic continent [*Hall and Visbeck*, 2002; *Lefebvre et al.*, 2004; *Lefebvre and Goosse*, 2005] plays an important role especially in setting the decadal time scale in the sea ice variability. More over, observational studies [*Behrendt et al.*, 2011; *Fahrbach et al.*, 2011] at the Weddell sea using hydrographic and mooring data shows local evidence of decadal fluctuations and interaction of warm subsurface water with the mixed layer and sea ice through upwelling and atmospheric change, although a global perspective could not applied due to the limited number of observation sections. Thus the oceanic variability through the long-term variability in the atmosphere drives the variability in the sea ice.

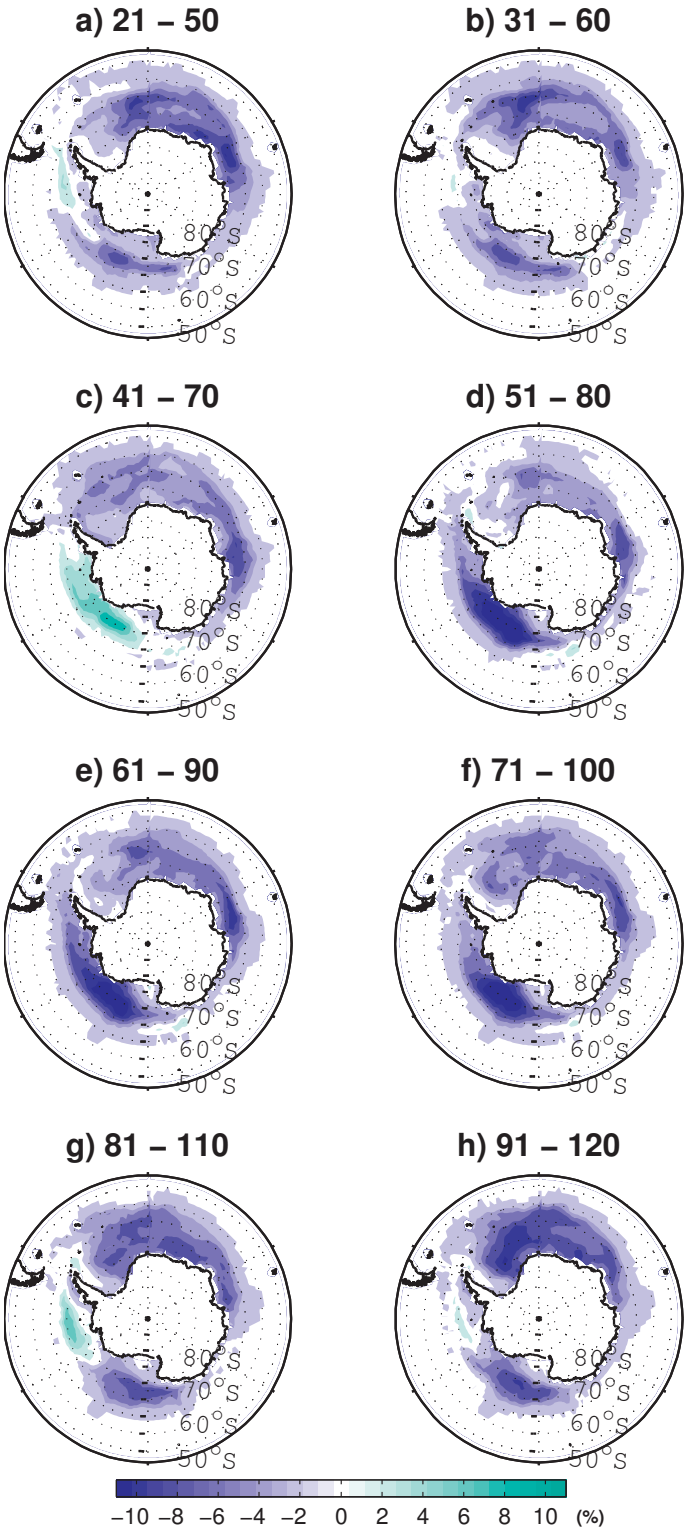

Figure 5.1: Spatial patterns of leading mode of annual mean sea ice concentration from the model derived from 30-year EOFs. a)-h) The figures represents different time series segments of 30 years with each title suggesting the time limit in years. The EOFs have been scaled by 1 standard deviation of the corresponding principal component time series to show the dimensional standard deviation at each grid point in the EOF.

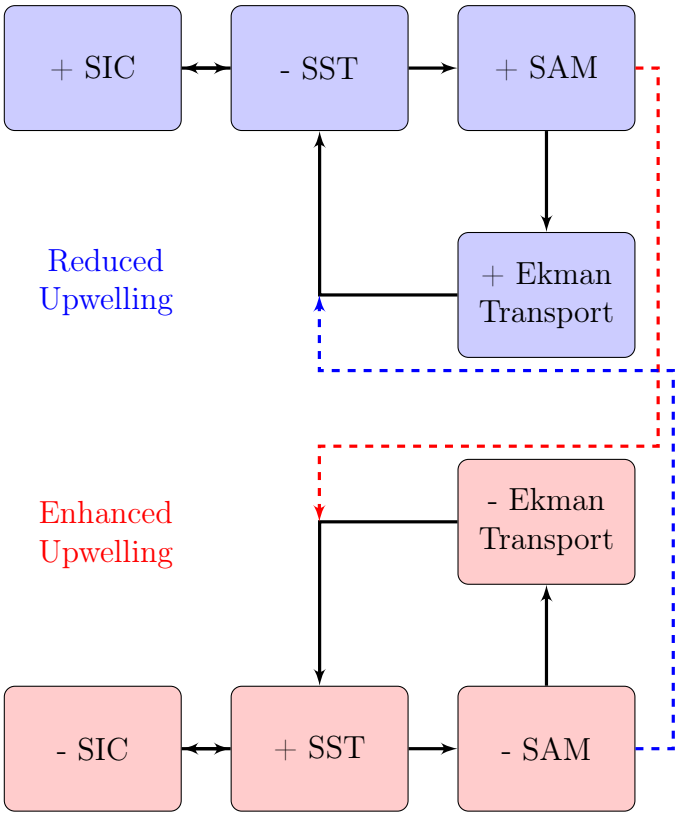

Figure 5.2: Schematic showing the role of ocean in setting the decadal time scale of the coupled variability of sea ice-ocean-atmosphere system.

Chapter 6

Conclusion

In this study we investigated the decadal variability of Antarctic sea ice using satellite observation and CGCM output data. The model showed good representation of the mean climatological fields and inter-annual variability in the sea ice and ocean. The patterns of inter-annual variability in the sea ice, SST and GPH were also simulated well in the model and hence used to study the decadal variability in the Antarctic sea ice.

Both the observation and model show a coupled circumpolar variabilty in a decadal time scale for the Antarctic sea ice. From observation data we obtained a decadal variability of 11-16 years in sea ice, 11-13 years in SST and 11-13 years in SAM. Similarly the model also showed a variability in the time scales of 12-17 years in sea ice, 11-13 years in SST and 11-12 years in SAM. The coupled relation can be summarized as, the long-term cooler (warmer) SST around the SIE corresponding to the positive (negative) SAM leads to increased (decreased) sea ice.

The CGCM revealed that the oceanic variability in the SST drives the variability

in the sea ice by setting the time scales by periodic decadal upwelling of warm sub-surface water. The upwelling periodicity was calculated to 14-18 years. The decadal SAM initiates the variability through change in wind (westerly) and ocean currents. The study results indicate that the SAM and oceanic variability are coupled through dynamic and thermodynamic feedback. Therefore, the impact on of oceanic natural decadal variability to the atmosphere is a key in the coupled system and has to be investigated upon further.

The decadal circumpolar variability described here is strongly manifested near the SIE, but it is possible that sea ice variability near the continent is also affected. A study shows 20 year cycle in break-up events of land fast-ice in summer and autumn at Lützow-Holm Bay in the Indian Ocean sector [*Ushio*, 2006], which largely influence the logistic conditions for the transport to the Antarctica. The break-up events hints at a decadal variability in the sea ice, which apart from the local forcings, longer-term variations in ocean through the atmospheric changes could be responsible. Therefore the feedback mechanisms on the longer timescale between ocean-ice-atmosphere have to be understood properly to predict future change in the Antarctic sea ice.

References

Behrendt, A., E. Fahrbach, M. Hoppema, G. Rohardt, O. Boebel, O. Klatt, A. Wisotzki, and H. Witte, 2011: Variations of Winter Water properties and sea ice along the Greenwich meridian on decadal time scales. *Deep. Sea Res. Part II: Top. Stud. Oceanogr.*, **58**, 2524–2532.

Capotondi, A., A. Wittenberg, and S. Masina, 2006: Spatial and temporal structure of Tropical Pacific interannual variability in 20th century coupled simulations. *Ocean Model.*, **15**, 274–298.

Cavalieri, D. J. and C. L. Parkinson, 2008: Antarctic sea ice variability and trends, 1979–2006. *J. Geophys. Res.*, **113**, 1–19.

Comiso, J., 2000: Bootstrap Sea Ice Concentrations from Nimbus–7 SMMR and DMSP SSM/I–SSMIS. Version 2. [1979–2010], Boulder, Colorado USA. National Snow and Ice Data Center.

Curry, J., J. Schramm, and E. Ebert, 1995: Sea ice–albedo climate feedback mechanism. *J. Clim.*, **8**, 240–247.

Dong, S., S. T. Gille, and J. Sprintall, 2007: An Assessment of the Southern Ocean Mixed Layer Heat Budget. *J. Clim.*, **20**, 4425–4442.

Fahrbach, E., M. Hoppema, G. Rohardt, O. Boebel, O. Klatt, and a. Wisotzki, 2011: Warming of deep and abyssal water masses along the Greenwich meridian on decadal time scales: The Weddell gyre as a heat buffer. *Deep. Sea Res. Part II: Top. Stud. Oceanogr.*, **58**, 2509–2523.

Gent, P. and J. Mcwilliams, 1990: Isopycnal mixing in ocean circulation models. *J. Phys. Oceanogr.*, **20**, 150–155.

Gong, D. and S. Wang, 1999: Definition of Antarctic Oscillation index. *Geophys. Res. Lett.*, **26**, 459.

Goosse, H., W. Lefebvre, A. Montety, E. Crespin, and A. H. Orsi, 2008: Consistent past half–century trends in the atmosphere, the sea ice and the ocean at high southern latitudes. *Clim. Dyn.*, **33**, 999–1016.

Hall, A. and M. Visbeck, 2002: Synchronous Variability in the Southern Hemisphere Atmosphere, Sea Ice, and Ocean Resulting from the Annular Mode*. *J. Clim.*, **15**, 3043–3057.

Holland, M. M., C. M. Bitz, and E. C. Hunke, 2005: Mechanisms Forcing an Antarctic Dipole in Simulated Sea Ice and Surface Ocean Conditions. *J. Clim.*, **18**, 2052–2066.

Holland, M. M., C. M. Bitz, and A. J. Weaver, 2001: The influence of sea ice physics on simulations of climate change. *J. Geophys. Res.*, **106**, 19 639.

Karoly, D., 1989: Southern Hemisphere circulation features associated with El Niño–Southern Oscillation events. *J. Clim.*, **2**, 1239–1252.

Komori, N., A. Kuwano-Yoshida, T. Enomoto, H. Sasaki, and W. Ohfuchi, 2008: High–Resolution Simulation of the Global Coupled Atmosphere–Ocean System: Description and Preliminary Outcomes of CFES (CGCM for the Earth Simulator). *High Resolution Numerical Modelling of the Atmosphere and Ocean*, K. Hamilton and W. Ohfuchi, Eds., Springer New York, chap. 14, 241–260.

Komori, N., K. Takahashi, K. Komine, T. Motoi, X. Zhang, and G. Sagawa, 2005: Description of sea–ice component of Coupled Ocean–Sea–Ice Model for the Earth Simulator (OIFES). *J. Earth Simulator.*, **4**, 31–45.

Kuwano-Yoshida, A., T. Enomoto, and W. Ohfuchi, 2010: An improved PDF cloud scheme for climate simulations. *Q. J. Royal Meteorol. Soc.*, **136**, 1583–1597.

Landrum, L., M. M. Holland, D. P. Schneider, and E. Hunke, 2012: Antarctic Sea Ice Climatology, Variability, and Late Twentieth–Century Change in CCSM4. *J. Clim.*, **25**, 4817–4838.

Lefebvre, W. and H. Goosse, 2005: Influence of the Southern Annular Mode on the sea ice–ocean system: the role of the thermal and mechanical forcing. *Ocean Sci. Discuss.*, **2**, 299–329.

Lefebvre, W., H. Goosse, R. Timmermann, and T. Fichefet, 2004: Influence of the Southern Annular Mode on the sea ice–ocean system. *J. Geophys. Res.*, **109**, C09 005.

Liu, J., J. A. Curry, and D. G. Martinson, 2004: Interpretation of recent Antarctic sea ice variability. *Geophys. Res. Lett.*, **31**, 2000–2003.

Marshall, G. J. and W. M. Connolley, 2006: Effect of changing Southern Hemisphere winter sea surface temperatures on Southern Annular Mode strength. *Geophys. Res. Lett.*, **33**, 1–4.

Numaguti, A., M. Takahashi, T. Nakajima, and A. Sumi, 1997: Description of CCSR/NIES Atmospheric General Circulation Model. Tech. rep., CGER's Supercomputer Monograph Report, Center for Global Environmental Reserch, National Institute for Environmental Studies, 1–48 pp.

Ohfuchi, W., et al., 2004: 10–km mesh meso–scale resolving simulations of the global atmosphere on the Earth Simulator – Preliminary outcomes of AFES (AGCM for the Earth Simulator). *J. Earth Simulator.*, **1**, 8–34.

Ohshima, K. I., et al., 2013: Antarctic Bottom Water production by intense sea–ice formation in the Cape Darnley polynya. *Nat. Geosci.*, **6**, 235–240.

Pacanowski, R. C. and S. Griffies, 1999: The MOM 3.0 manual. Tech. rep., GFDL Ocean Group Technical Report 4, NOAA/Geophysical Fluid Dynamics Laboratory, Princeton, NJ, U.S.A.

Parkinson, C. L. and D. J. Cavalieri, 2012: Antarctic sea ice variability and trends, 1979–2010. *The Cryosphere.*, **6**, 871–880.

Redi, M., 1982: Oceanic isopycnal mixing by coordinate rotation. *J. Phys. Oceanogr.*, **12**, 1154–1158.

Reynolds, R., 1988: A real–time global sea surface temperature analysis. *J. climate.*, **1**, 75–86.

Reynolds, R. and D. Marsico, 1993: An improved real–time global sea surface temperature analysis. *J. climate.*, **6**, 114–119.

Reynolds, R. W., N. A. Rayner, T. M. Smith, D. C. Stokes, and W. Wang, 2002: An improved in situ and satellite SST analysis for climate. *J. Clim.*, **15**, 1609–1625.

Richter, I., S. K. Behera, Y. Masumoto, B. Taguchi, N. Komori, and T. Yamagata, 2010: On the triggering of Benguela Niños: Remote equatorial versus local influences. *Geophys. Res. Lett.*, **37**, 1–6.

Sen Gupta, A. and M. H. England, 2006: Coupled Ocean–Atmosphere–Ice Response to Variations in the Southern Annular Mode. *J. Clim.*, **19**, 4457–4486.

Stammerjohn, S. E., D. G. Martinson, R. C. Smith, X. Yuan, and D. Rind, 2008: Trends in Antarctic annual sea ice retreat and advance and their relation to El Niño–Southern Oscillation and Southern Annular Mode variability. *J. Geophys. Res.*, **113**, 1–20.

Taguchi, B., H. Nakamura, M. Nonaka, N. Komori, A. Kuwano-Yoshida, K. Takaya, and A. Goto, 2012: Seasonal Evolutions of Atmospheric Response to Decadal SST Anomalies in the North Pacific Subarctic Frontal Zone: Observations and a Coupled Model Simulation. *J. Clim.*, **25**, 111–139.

Thompson, D. and J. Wallace, 2000: Annular Modes in the Extratropical Circulation. Part I: Month–to–Month Variability. *J. Clim.*, **13**, 1000–1016.

Thompson, D. W. J. and S. Solomon, 2002: Interpretation of recent Southern Hemisphere climate change. *Sci.*, **296**, 895–9.

Thompson, D. W. J., J. M. Wallace, and G. C. Hegerl, 2000: Annular Modes in the Extratropical Circulation. Part II: Trends. *J. Clim.*, **13**, 1018–1036.

Turner, J., T. J. Bracegirdle, T. Phillips, G. J. Marshall, and J. S. Hosking, 2013: An Initial Assessment of Antarctic Sea Ice Extent in the CMIP5 Models. *J. Clim.*, **26**, 1473–1484.

Udagawa, Y., Y. Tachibana, and K. Yamazaki, 2009: Modulation in interannual sea ice patterns in the Southern Ocean in association with large–scale atmospheric mode shift. *J. Geophys. Res.*, **114**, 1–12.

Ushio, S., 2006: Factors affecting fast–ice break–up frequency in Lützow–Holm Bay, Antarctica. *Annals Glaciol.*, **44**, 177–182.

Visbeck, M., 2009: A Station–Based Southern Annular Mode Index from 1884 to 2005. *J. Clim.*, **22**, 940–950.

Walsh, J. E., 1983: The role of sea ice in climatic variability: Theories and evidence 1. *Atmosphere-Ocean.*, **21**, 229–242.

White, W. B. and R. G. Peterson, 1996: An Antarctic circumpolar wave in surface pressure, wind, temperature and sea–ice extent. *Nat.*, **380**, 699–702.

Yuan, X., 2004: ENSO–related impacts on Antarctic sea ice: a synthesis of phenomenon and mechanisms. *Antarctic Sci.*, **16**, 415–425.

Yuan, X. and C. Li, 2008: Climate modes in southern high latitudes and their impacts on Antarctic sea ice. *J. Geophys. Res.*, **113**, 1–13.

Yuan, X. and D. G. Martinson, 2000: Antarctic Sea Ice Extent Variability and Its Global Connectivity*. *J. Clim.*, **13**, 1697–1717.

Yuan, X. and E. Yonekura, 2011: Decadal variability in the Southern Hemisphere. *J. Geophys. Res.*, **116**, 1–12.

Zhang, X. and J. Zhang, 2001: Heat and freshwater budgets and pathways in the Arctic Mediterranean in a coupled ocean/sea–ice model. *J. oceanography.*, **57**, 207–234.

Zunz, V., H. Goosse, and F. Massonnet, 2013: How does internal variability influence the ability of CMIP5 models to reproduce the recent trend in Southern Ocean sea ice extent? *The Cryosphere.*, **7**, 451–468.

Zwally, H. J., Josefino C. Comiso, Claire L. Parkinson, Donald J. Cavalieri, and Per Gloersen, 2002: Variability of Antarctic sea ice 1979–1998. *J. Geophys. Res.*, **107**, 3041.

Acknowledgments

First and foremost, I would like to express my humble, heartfelt and deepest gratitude to my research supervisor Dr. Shigeru Aoki, for his guidance, suggestions and encouragement. Without his persistent support and incredible patience towards me, this dissertation would not have happened.

I would like to thank and acknowledge the help provided by Dr. Guy Williams, Dr. Shimada Keishi and Dr. Sohey Nihashi during the starting day of my PhD work. Thanks to all the professors and colleagues of our group for their continuous support. My special thanks to Ms. Kyoko Kitagawa, our group secretary for helping me out in all official and unofficial works.

My "Thank You" to all my friends for their understanding, support, care and timely helps.

The provision of Sea ice data by the National Snow and Ice Data Center (NSIDC), OI_SST_V2 by Earth System Research Laboratory (ESRL), NOAA and Antarctic Oscillation index by Climate Prediction Center, NOAA/NCEP are gratefully acknowledged. The integration of the CFES was carried out on the Earth Simulator under the support of JAMSTEC.

I would like to thank the Japanese people for their kindness and hospitality and Japanese Government from providing financial support thorough Ministry of Education, Culture, Sports, Science and Technology (MEXT) scholarship.

Finally, I express my profound gratitude for my papa and mummy who are always there for me with their love, affection, prayers and blessings.